


Article

Adaptive Global Fast Sliding Mode Control for Steer-by-Wire System Road Vehicles

Junaid Iqbal ¹ , Khalil Muhammad Zuhaib ¹, Changsoo Han ^{2,*}, Abdul Manan Khan ² and Mian Ashfaq Ali ³

¹ Department of Mechatronics Engineering, Hanyang University ERICA Campus, Ansan 15588, Korea; jibssp@gmail.com (J.I.); kmzuhaib@gmail.com (K.M.Z.)

² Department of Robot Engineering, Hanyang University ERICA Campus, Ansan 15588, Korea; kam@hanyang.ac.kr

³ School of Mechanical and Manufacturing Engineering (SMME), National University of Science and Technology (NUST), Islamabad 44000, Pakistan; ishfaqaries@gmail.com

* Correspondence: cshan@hanyang.ac.kr; Tel.: +82-31-400-4062

Academic Editor: Felipe Jimenez

Received: 21 June 2017; Accepted: 13 July 2017; Published: 19 July 2017

Abstract: A steer-by-wire (SbW) system, also known as a next-generation steering system, is one of the core elements of autonomous driving technology. Navigating a SbW system road vehicle in varying driving conditions requires an adaptive and robust control scheme to effectively compensate for the uncertain parameter variations and external disturbances. Therefore, this article proposed an adaptive global fast sliding mode control (AGFSMC) for SbW system vehicles with unknown steering parameters. First, the cooperative adaptive sliding mode observer (ASMO) and Kalman filter (KF) are established to simultaneously estimate the vehicle states and cornering stiffness coefficients. Second, based on the best set of estimated dynamics, the AGFSMC is designed to stabilize the impact of nonlinear tire-road disturbance forces and at the same time to estimate the uncertain SbW system parameters. Due to the robust nature of the proposed scheme, it can not only handle the tire-road variation, but also intelligently adapts to the different driving conditions and ensures that the tracking error and the sliding surface converge asymptotically to zero in a finite time. Finally, simulation results and comparative study with other control techniques validate the excellent performance of the proposed scheme.

Keywords: adaptive global fast sliding mode (AGFSM); adaptive sliding mode observer (ASMO); Kalman filter (KF); Steer-by-Wire (SbW)

1. Introduction

The automobile industry is immensely working to transform conventional road vehicles into partial/full autonomous vehicles. SAE International and NHTSA have classified six levels of driving autonomy from “no automation” to “full automation” [1,2]. In particular, from the lane-keeping assistance system [3] to fully automated maneuvering [4–6], Steer-by-Wire (SbW) technology is playing a fundamental role in advanced driving assistance systems [7]. Nissan introduced the first commercialized SbW system in 2013 with the Infiniti Q50 vehicle [8,9]. The SbW system delivers better overall steering performance with comfort, reduces power consumption, provides active steering control, and significantly improves the passenger safety. Compared with a conventional steering system, the SbW system has replaced the mechanical shaft between the steering wheel and front wheels with two actuators, controllers, and sensors. The first actuator steers the front wheels and the second actuator provides steering feel feedback to the driver, obtained from the road and tire dynamics.

Over the last decade, many researchers have proposed a number of control techniques to compensate for the system parameter variation, change in road conditions, and external disturbances for obtaining the robust performance of the SbW system. In [10,11], sliding mode based control schemes are proposed for a partially known SbW system with unknown lumped uncertainties to track the reference signal. However, it is hard to classify the wide range of nominal parameters under the sideslip, and the robust performance may not be guaranteed over different road conditions. In [12–16], the upper bound sliding mode control (SMC) technique is proposed for the bounded unknown SbW system parameters and uncertain dynamics. However, the process of obtaining these proper bounds is not evident. In [17–20] proportional-derivative (PD) control is proposed to follow the driver's steering wheel signal closely. However, under uncertain dynamics, it is difficult to achieve satisfactory performance with a conventional control scheme. In [21] cornering stiffness and chassis side slip angle are estimated to calculate the self-aligning torque. The authors used the proportion of estimated torque as a feedback to the driver for artificial steering feel. In [22] three suboptimal sliding mode techniques are evaluated for yaw-rate tracking problem in over-actuated vehicles. In [23,24], adaptive control is implemented for path tracking via SbW system and the authors estimated the sliding gains by considering the known steering parameters and cornering coefficients. However, they did not use any mechanism to stop the estimation. Consequently, the controller could lead to saturation by estimating too large a sliding gain. In [25,26] the authors proposed a hyperbolic tangent function with adaptive SMC based schemes to counter the effect of self-aligning torque. In [27] the frictional torque and self-aligning torque are replaced by a second-order polynomial function that acts as an external disturbance over the SbW system. The authors proposed an adaptive terminal SMC (ATSMC) to estimate the upper bounds of parameters and disturbance.

Apart from the control design, a robust estimation methodology is also needed for the SbW system to estimate the vehicle states, uncertain parameters, and tire–road conditions for eliminating the effect of external disturbances from the controller. For instance, in recent years Kalman filter (KF) and nonlinear observers have gained much more attention from researchers; for example, in [28] a dual extended KF is used to estimate vehicle states and road friction. In [29] the authors estimated five DOF vehicle states and inertial parameters, such as overloaded vehicle's additional mass, respective yaw moment of inertia, and its longitudinal position using the dual unscented KF by considering the constant road–tire friction over a flat road. In [30–32] a fixed gain based full-state nonlinear observer is designed to estimate the longitudinal, lateral, and yaw velocities of the vehicle. However, for good estimation performance the observer gains must be tuned to a wide range of driving conditions. In order to reduce the burden of gain tuning from a nonlinear observer [33], employed linear matrix inequality based convex optimization to obtain the gains of reduced order observer for estimating vehicle velocities. In [34] the authors implemented an adaptive gain based sliding mode observer to estimate the battery's charging level and health in electric vehicles.

In this paper first, we have established the adaptive sliding mode observer (ASMO) and the Kalman filter (KF) to simultaneously estimate the vehicle states and cornering stiffness coefficients by using the yaw rate and the strap down [35] lateral acceleration signals. Then, based on the simultaneously estimated dynamics, the two-fold adaptive global fast sliding mode control (AGFSMC) is designed for SbW system vehicles, considering that the steering parameters are unknown. In the first fold, estimated dynamics-based control (EDC) is utilized to stabilize the impact of self-aligning torque and frictional torque. In the second fold, the AGFSMC is developed to estimate the uncertain SbW parameters and eliminate the effect of residual disturbance left out from the EDC. The adaptation capability of the proposed scheme not only intelligently handles the tire–road environmental changes, but also adapts the system parameters and sliding gains according to the different driving conditions.

Finally, for avoiding overestimations of parameters and gains, discontinuous projection mapping [36] is incorporated to stop the estimation and adaptive mechanism as the tracking error converges to the designed dead zone bounds [37]. In the simulated results section, the comparative

study will show the effectiveness of the proposed AGFSMC scheme, which ensures that the tracking error and sliding surface converge asymptotically to zero in a finite time.

The rest of the paper is structured as follows: In Sections 2 and 3, vehicle dynamics modeling and SbW system modeling with external disturbance are discussed. In Section 4, the ASMO and KF are established to estimate the vehicle states and parameters. In Section 5, the AGFSMC scheme is developed for the SbW system and the convergence analysis with bounded conditions is discussed in detail. Section 6 describes the simulation results and findings to validate the proposed scheme, followed by the last section that concludes the paper.

2. Vehicle Dynamics Modeling

Figure 1 illustrates the simplest bicycle model of a vehicle, which has a central front wheel and a central rear wheel, in place of two front and two rear wheels. The vehicle has two degrees of freedom, represented by the lateral motion y and the yaw angle ψ . According to Figure 1, the dynamics along the y axis and yaw axis are described as [38,39]:

$$m(\ddot{y} + V_x \dot{\psi}) = F_{yf} \cos \delta_{fw} + F_{xf} \sin \delta_{fw} + F_{yr} \quad (1)$$

$$I_z \ddot{\psi} = l_f (F_{yf} \cos \delta_{fw} + F_{xf} \sin \delta_{fw}) - l_r F_{yr}, \quad (2)$$

where \ddot{y} , $\dot{\psi}$, and $\ddot{\psi}$ are the acceleration with respect to the y axis motion, yaw rate, and yaw acceleration, respectively. l_f and l_r represent the distance of front and rear axles from the center of gravity, respectively. m and I_z are the mass of vehicle and the moment of inertia along the yaw axis, respectively. V_x denotes the longitudinal vehicle velocity at the center of gravity. F_{xf} and F_{xr} are the longitudinal forces of the front and rear wheels, respectively. F_{yf} and F_{yr} are the lateral frictional forces of front and rear wheels, respectively, as shown in Figure 1.

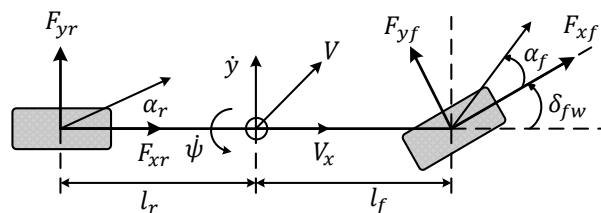


Figure 1. Bicycle model of vehicle.

In order to simplify the model, it is assumed that longitudinal forces F_{xf} , F_{xr} are equal to zero and by using the small angle approximation, i.e., $\cos \delta_{fw} \approx 1$, the simplified dynamics can be modeled as follows:

$$m(\ddot{y} + V_x \dot{\psi}) = F_{yf} + F_{yr} \quad (3)$$

$$I_z \ddot{\psi} = l_f F_{yf} - l_r F_{yr}. \quad (4)$$

For small slip angles, the lateral frictional forces are proportional to slip-angle α_f and α_r at the front and rear wheels, respectively. Therefore, lateral forces are defined as:

$$F_{yf} = 2C_f \alpha_f \quad (5)$$

$$F_{yr} = 2C_r \alpha_r, \quad (6)$$

where

$$\alpha_f = \delta_{fw} - \frac{V_y + l_f \dot{\psi}}{V_x} \quad (7)$$

$$\alpha_r = -\frac{V_y - l_f \dot{\psi}}{V_x}, \quad (8)$$

where C_f and C_r are the front and rear tires' cornering stiffness coefficients. δ_{fw} denotes the steering angle of front wheels, which is considered the same for both front wheels, and factor 2 accounts for two front and two rear wheels, respectively.

By using the small angle approximation $V_y = \dot{y}$ [38], Equations (7) and (8) can be written as:

$$\alpha_f = \delta_{fw} - \frac{\dot{y} + l_f \dot{\psi}}{V_x} \quad (9)$$

$$\alpha_r = -\frac{\dot{y} - l_r \dot{\psi}}{V_x}. \quad (10)$$

Substituting Equations (5), (6), (9) and (10) into Equations (3) and (4), the state space model is represented as:

$$\dot{x} = Ax + B\delta_{fw}, \quad (11)$$

where

$$x = [\dot{y} \dot{\psi}]^T$$

$$A = \begin{bmatrix} -2\left(\frac{C_f + C_r}{mV_x}\right) & -\left(V_x + 2\left(\frac{l_f C_f - l_r C_r}{mV_x}\right)\right) \\ -2\left(\frac{l_f C_f - l_r C_r}{I_z V_x}\right) & -2\left(\frac{l_f^2 C_f + l_r^2 C_r}{I_z V_x}\right) \end{bmatrix}, B = \begin{bmatrix} \frac{2C_f}{m} \\ \frac{2l_f C_f}{I_z} \end{bmatrix}. \quad (12)$$

3. Steer-by-Wire System Modeling

Figure 2 depicts the standard model of SbW system for road vehicles. As shown, the steering wheel angle sensor is used to detect the driver's reference angle and the feedback motor is used to provide the artificial steering feel.

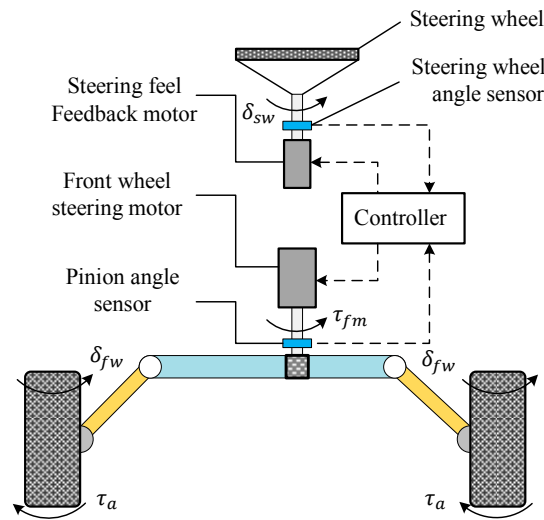


Figure 2. Steer-by-wire model.

Similarly, the front wheel angle is detected by the pinion angle sensor. Based on the error between the reference angle and the front wheel angle, the control signal is provided to the front wheel steering motor to closely steer the front wheels according to the driver's reference angle.

The equivalent second-order dynamics of the front wheels' steering motor is expressed as follows [10,15]:

$$J_{eq}\ddot{\delta}_{fw} + B_{eq}\dot{\delta}_{fw} + \tau_F + \tau_a = ku, \quad (13)$$

where J_{eq} and B_{eq} are the equivalent moment of inertia and the equivalent damping of the SbW system, respectively. u is the front wheels' steering motor control input and k is the steering ratio between the steering wheel angle and the front wheels' angle, given by $\delta_{fw} = \delta_{sw}/k$.

It is known that many modern road vehicles use the variable steering ratio. Therefore, dividing both sides of Equation (13) by k eliminates the impact of the variable steering ratio from the proposed control scheme without compromising the steering performance. Thus, the dynamics of SbW system can be written as:

$$J_{ek}\ddot{\delta}_{fw} + B_{ek}\dot{\delta}_{fw} + \tau_{Fk} + \tau_{ak} = u, \quad (14)$$

where

$$J_{ek} = \frac{J_{eq}}{k} = \frac{J_{fw}}{k} + J_{fm}k \quad (15)$$

$$B_{ek} = \frac{B_{eq}}{k} = \frac{B_{fw}}{k} + B_{fm}k \quad (16)$$

$$\tau_{Fk} = \frac{\tau_F}{k} \quad (17)$$

$$\tau_{ak} = \frac{\tau_a}{k}, \quad (18)$$

where J_{fw} and J_{fm} are the moment of inertia of the front wheels and the front wheel steering motor, respectively. B_{fw} and B_{sm} are the damping factors of the front wheels and the front wheel steering motor, respectively.

When the vehicle is turning, the steering system experiences torque that tends to resist the attempted turn, known as self-aligning torque τ_a . It can be seen from Figure 3 that the resultant lateral force developed by the tire manifests the self-aligning torque. The lateral force is acting behind the tire center on the ground plane and tries to align the wheel plane with the direction of wheel travel. Therefore, the total self-aligning torque is given by [14]:

$$\tau_a = F_{yf}(t_p + t_m), \quad (19)$$

where t_p is the pneumatic trail (the distance between the application point of lateral force F_{yf} to the center of tire), t_m is the mechanical trail, also known as the caster offset, which is the distance between the tire center and the point where the steering axis intersects with the ground plane.

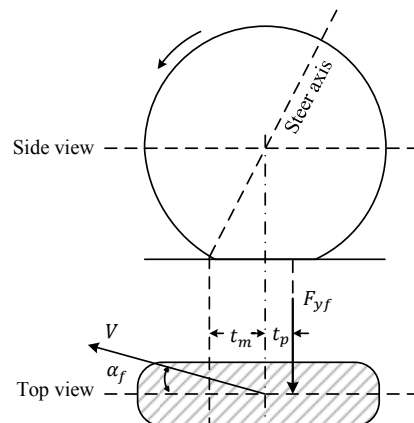


Figure 3. Self-aligning torque on front wheel.

By substituting Equations (5) and (9) into Equation (19), τ_a can be written as:

$$\tau_a = 2C_f \left(\delta_{fw} - \frac{\dot{y} + l_f \dot{\psi}}{V_x} \right) (t_p + t_m). \quad (20)$$

Moreover, τ_F is the coulomb frictional torque acting on SbW system, expressed as [23]:

$$\tau_F = F_{zf} \mu t_p \text{sign}(\dot{\delta}_{fw}) \quad (21)$$

$$F_{zf} = \frac{mg l_r}{l_f + l_r}, \quad (22)$$

where F_{zf} is the normal load on front axle, μ is the coefficient of friction, mg is the vehicle's weight without any external load, and $\text{sign}()$ signum function is used to identify the direction of the frictional torque.

The stability of the SbW system mainly depends on the road and environmental conditions. The uncertain road surface such as dry, wet, or icy can produce considerable variations in the tire cornering stiffness coefficients C_f , C_r , which can adversely affect the controller performance. Therefore, to estimate the vehicle states and the uncertain parameter variation, the cooperative ASMO and KF are designed in the next section.

4. ASMO and KF

In this section, we will first design the ASMO for yaw rate $\dot{\psi}$ and lateral velocity \dot{y} , and then use the KF parameter estimator to estimate the tire cornering stiffness coefficients under varying road conditions.

In order to design the observer, a few assumptions are made, such as: the yaw rate $\dot{\psi}$ is directly measurable from yaw rate sensor; and the vehicle's longitudinal velocity is obtained from $V_x = r_e \omega$, where r_e is the effective tire radius and ω is the averaged free wheels angular speed measured from the wheel encoders. Moreover, it is considered that there is no effect of gravitation acceleration g on the lateral acceleration a_y , such that the a_y measurement model is defined as [29]:

$$a_{y,sensor} = \ddot{y} + V_x \dot{\psi}. \quad (23)$$

Therefore, the lateral velocity can be obtained from a strapdown algorithm [35] as follows:

$$\dot{y}(t) = \dot{y}(t-1) + \int (a_{y,sensor} - V_x \dot{\psi}) dt, \quad (24)$$

where $\dot{y}(t-1)$ is the prior lateral velocity.

The conventional sliding mode observer (SMO) for vehicle states (Equation (11)) can be designed as:

$$\ddot{\hat{y}} = -A_{11}\dot{\hat{y}} - A_{12}\dot{\hat{\psi}} + B_1\delta_{fw} + L_1\text{sign}(\dot{y} - \dot{\hat{y}}) \quad (25)$$

$$\ddot{\hat{\psi}} = -A_{21}\dot{\hat{y}} - A_{22}\dot{\hat{\psi}} + B_2\delta_{fw} + L_2\text{sign}(\dot{\psi} - \dot{\hat{\psi}}), \quad (26)$$

where A_{11} , A_{12} , B_1 , and B_2 are the elements of Equation (12) with nominal m_0 and I_{z0} ; L_1 and L_2 are the observer gains, which must satisfy the following conditions, such that:

$$L_1 > \max(|A_{11}e_1| + |A_{12}e_2|) \quad (27)$$

$$L_2 > \max(|A_{12}e_1| + |A_{22}e_2|), \quad (28)$$

where $e_1 = \dot{y} - \dot{\hat{y}}$ and $e_2 = \dot{\psi} - \dot{\hat{\psi}}$.

The road surface variation is a critical factor for tuning the observer gains L_1 and L_2 during the design process. Any inappropriate selection of L_1 and L_2 will significantly reduce the SMO performance, resulting in a possible deviation of state estimation from the original trajectory.

Due to the aforementioned fact, an adaptive gain based sliding mode observer [34] is proposed, which improves the estimation performance by adapting the observer gains according to tire road conditions. Therefore, Equations (25) and (26) are changed to new forms, as follows:

$$\ddot{\hat{y}} = -A_{11}\dot{\hat{y}} - A_{12}\dot{\hat{\psi}} + B_1\delta_{fw} + \hat{L}_1(t)\text{sign}(e_1) \quad (29)$$

$$\ddot{\hat{\psi}} = -A_{21}\dot{\hat{y}} - A_{22}\dot{\hat{\psi}} + B_2\delta_{fw} + \hat{L}_2(t)\text{sign}(e_2), \quad (30)$$

where the ASMO gain adaptation law for $i = 1, 2$ is expressed as:

$$\dot{\hat{L}}_i(t) = \begin{cases} \rho_i |e_i|, & |e_i| > \varepsilon_i \\ 0, & \text{otherwise} \end{cases} \quad (31)$$

where $\hat{L}_i(t) > 0$, is strictly positive time varying adaptive ASMO gain. ρ_i is a positive scalar used to adjust the adaption speed. $\varepsilon_i \ll 1$ are small positive constants used to activate the adaptation mechanism with the condition defined in Equation (31); therefore, as the error converges to the bound $|e_i| \leq \varepsilon_i$ in finite time, $\hat{L}_i(t)$ will stop increasing.

For convergence proof, the Lyapunov function of ASMO for lateral velocity is defined as:

$$V_1 = \frac{1}{2}e_1^2 + \frac{1}{2\rho_1}\tilde{L}_1, \quad (32)$$

where $\tilde{L}_1 = \hat{L}_1 - L_1$ is the adaptive gain convergence error.

The derivative of V_1 , with the consideration that $\dot{\hat{L}}_1 = 0$, is obtained as follows:

$$\begin{aligned} \dot{V}_1 &= e_1\dot{e}_1 + \frac{1}{\rho_1}\tilde{L}_1\dot{\hat{L}}_1 \\ &= e_1[-A_{11}e_1 - A_{12}e_2 - \hat{L}_1\text{sign}(e_1)] + \frac{1}{\rho_1}\tilde{L}_1\dot{\hat{L}}_1 \\ &\leq e_1[-A_{11}e_1 - A_{12}e_2] - \hat{L}_1|e_1| + (\hat{L}_1 - L_1)|e_1| \\ &\leq e_1[-A_{11}e_1 - A_{12}e_2] - L_1|e_1|. \end{aligned} \quad (33)$$

Thus, by considering Equation (27):

$$\dot{V}_1 \leq 0. \quad (34)$$

Similarly, the Lyapunov function V_2 for yaw rate convergence error e_2 and adaptive gain convergence error $\tilde{L}_2 = \hat{L}_2 - L_2$ can be written as:

$$V_2 = \frac{1}{2}e_2^2 + \frac{1}{2\rho_2}\tilde{L}_2. \quad (35)$$

The time derivative of Equation (35) will asymptotically converge to zero, $\dot{V}_2 \leq 0$, by considering $\dot{L}_2 = 0$ and $L_2 > \max(|a_{12}e_1| + |a_{22}e_2|)$.

Remark 1. In the practical implementation, the direct strapdown of lateral acceleration may incorporate the small continuous noise to the lateral velocity that can diverge the ASMO estimation over time. Therefore, to deal with the issue, a lateral velocity-based damping term [40] is added to cancel out the incremental noise. Now Equation (24) can be written as:

$$\dot{y}(t) = \dot{y}(t-1)(1-\sigma) + \int (a_{y,sensor} - V_x\dot{\psi})dt, \quad (36)$$

where $\sigma > 0$ is an adjustable small damping parameter.

Remark 2. The designed ASMO may encounter high-frequency chattering due to the discontinuous signum function $\text{sign}()$; therefore, it is replaced by the continuous function $e_i / (|e_i| + \varepsilon_i)$, such that Equations (29) and (30) are rewritten as:

$$\ddot{y} = -A_{11}\dot{y} - A_{12}\dot{\psi} + B_1\delta_{fw} + \hat{L}_1(t) \frac{e_1}{|e_1| + \varepsilon_1} \quad (37)$$

$$\ddot{\psi} = -A_{21}\dot{y} - A_{22}\dot{\psi} + B_2\delta_{fw} + \hat{L}_2(t) \frac{e_2}{|e_2| + \varepsilon_2}. \quad (38)$$

The estimation performance of the ASMO for lateral velocity and yaw rate primarily depends upon the knowledge of tire cornering stiffness coefficients C_f and C_r , which are unknown in practice and cannot be measured directly from the onboard vehicle sensors. Therefore, a Kalman filter (KF) [41] is proposed in cooperation with ASMO to estimate these stiffness coefficients under different tire–road conditions. Once the KF estimates a sufficient set of tire cornering stiffness coefficients, the parameter estimation can be switched off.

The KF algorithm [41] for tire cornering stiffness estimation is given in Table 1.

Table 1. Kalman filter algorithm.

1. Initialize \hat{w}_0, P_0:
$\hat{w}_0 = E[w(0)]$
$P_0 = E[(w(0) - \hat{w}_0)(w(0) - \hat{w}_0)^T]$
2. Time Update:
$\hat{w}_t^- = \hat{w}_{t-1}$
$P_t^- = P_{t-1} + Q$
3. Measurement Update:
$K_t = P_t^- H^T (H P_t^- H^T + R)^{-1}$
$\hat{w}_t = \hat{w}_t^- + K_t(z_t - H\hat{w}_t^-)$
$P_t = (I - K_t H) P_t^-$

P denotes the estimate error covariance, Q is the process noise covariance, and $R = r_s^2$ is the measurement noise covariance, whereas r_s represents the sensor's zero-mean white noise.

The tire cornering coefficients vector w and the measurement z , consisting of the lateral acceleration a_y , are defined as:

$$w = [C_f \ C_r]^T, z = Hw, \quad (39)$$

where

$$H = \left[-\frac{2}{m_0} \left(\frac{\dot{y} + l_f \dot{\psi}}{V_x} - \delta_{fw} \right) - \frac{2}{m_0} \left(\frac{\dot{y} - l_r \dot{\psi}}{V_x} \right) \right]. \quad (40)$$

It is to be noted that the tire cornering stiffness coefficient's vector w is considered as constant, therefore, the time derivative of w is zero, ($\dot{w} = 0$). Then, w and z can be written in Euler's discretized form as:

$$w(k) = w(k-1) + v(k) \quad (41)$$

$$z(k) = Hw(k) + r(k), \quad (42)$$

where v and r are the zero mean process noise and measurement noise, respectively.

In order to improve the estimation performance and the convergence accuracy of KF, the difference $e_3 = z_t - H\hat{w}_t^-$, known as residual, is utilized to switch off the KF estimator. Therefore, on the basis of

e_3 , a bounded condition is selected, such that when e_3 reaches the specified bound $|e_3| \leq \varepsilon_3$, the KF will stop the estimation process and thereafter the estimated parameters will become constant until e_3 exceeds the specified condition. ε_3 ($\varepsilon_3 > 0$) is the small positive constant.

Thus, the estimated tire cornering stiffness-based ASMO for Equations (37) and (38) is revised as:

$$\ddot{\hat{y}} = -A_{11}(\hat{w}_{t-1})\dot{\hat{y}} - A_{12}(\hat{w}_{t-1})\dot{\hat{\psi}} + B_1(\hat{w}_{t-1})\delta_{fw} + \hat{L}_1(t)\frac{e_1}{|e_1| + \varepsilon_1} \quad (43)$$

$$\ddot{\hat{\psi}} = -A_{21}(\hat{w}_{t-1})\dot{\hat{y}} - A_{22}(\hat{w}_{t-1})\dot{\hat{\psi}} + B_2(\hat{w}_{t-1})\delta_{fw} + \hat{L}_2(t)\frac{e_2}{|e_2| + \varepsilon_2}. \quad (44)$$

5. AGFSMC Control Design

In this section, the estimated dynamics-based adaptive global fast sliding mode control (AGFSMC) is designed in two steps to estimate the uncertain steering parameters and eliminate the effect of varying tire–road disturbance forces, so that the front wheels asymptotically track the driver’s reference command in finite time.

The tracking error e_θ between the front wheel angle δ_{fw} and the scaled reference hand wheel angle δ_d is defined as:

$$e_\theta(t) = \delta_{fw}(t) - \frac{\delta_{sw}(t)}{k} = \delta_{fw}(t) - \delta_d(t). \quad (45)$$

The combination of linear sliding surface and the terminal sliding surface is known as the global fast terminal sliding surface, s , which is defined as [42]:

$$s = \dot{e}_\theta + \lambda_1(e_\theta)^{q/p} + \lambda_2 e_\theta, \quad (46)$$

where λ_1 and λ_2 ($\lambda_1, \lambda_2 > 0$), are strictly positive constants, and q and p , are positive odd numbers, such that $q < p$.

Thus, the time derivative of s is obtained as:

$$\dot{s} = \ddot{e}_\theta + \lambda_1 \frac{q}{p} (e_\theta)^{\frac{q}{p}-1} \dot{e}_\theta + \lambda_2 \dot{e}_\theta. \quad (47)$$

\dot{s} can be written as:

$$\dot{s} = \ddot{\delta}_{fw} - \ddot{\delta}_r, \quad (48)$$

where $\ddot{\delta}_r$ is expressed as:

$$\ddot{\delta}_r = \ddot{\delta}_d - \left(\lambda_1 \frac{q}{p} (e_\theta)^{\frac{q}{p}-1} + \lambda_2 \right) \dot{e}_\theta. \quad (49)$$

Thus, for stabilizing the SbW system (Equation (14)) and exponentially converging the tracking error (Equation (45)) to zero, the two-step closed loop control law u for the SbW system is designed as:

$$u = u_E + u_A, \quad (50)$$

where, in the first step, the estimated dynamics based control (EDC) u_E , is designed to counter the tire–road disturbance acting on the SbW system as follows:

$$u_E = -\text{sign}(s)(|\xi\tau_{ak}| + |\xi\tau_{Fk}|), \quad (51)$$

where $\xi\tau_{ak}$, is the estimated self-aligning torque, which is computed from the best set of estimated vehicle states and front wheel cornering stiffness provided by the ASMO and KF. $\xi\tau_{Fk}$ is the nominal frictional torque obtained from the nominal set of vehicle parameters, such as mass, nominal coefficient of friction, and the geometry of the vehicle.

Both $|\zeta\tau_{ak}|$ and $|\zeta\tau_{Fk}|$ are expressed as:

$$|\zeta\tau_{ak}| = \frac{2\hat{C}_f}{k_0}(t_{p_0} + t_m) \left| \left(\delta_{fw} - \frac{\dot{y} + l_f \dot{\psi}}{V_x} \right) \right| \quad (52)$$

$$|\zeta\tau_{Fk}| = \frac{m_0 g l_r}{(l_f + l_r)k_0} \mu_0 t_{p_0} |\text{sign}(\dot{\delta}_{fw})|, \quad (53)$$

where \dot{y} , $\dot{\psi}$, and \hat{C}_f are the observed vehicle states and the front wheel's estimated cornering stiffness, as worked out in the previous section, respectively. μ_0 , t_{p_0} , m_0 , and k_0 are the nominal system parameters.

Second, to tackle the residual disturbance left by the EDC and estimate the uncertain steering parameters, the adaptive global fast sliding mode control (AGFSMC) u_A is designed as follows:

$$u_A = -\text{sign}(s) \left(|y|\hat{a} + \hat{\tau} \left| \frac{\dot{y} + l_f \dot{\psi}}{V_x} \right| + \hat{\beta}_1 |u(t-1)| \right) - \beta_2 s, \quad (54)$$

where $\hat{a}(t)$ is the estimated parameter's vector and $|y|$ is the signal feedback vector; they are defined as follows:

$$\hat{a} = [\hat{J}_{ek} \hat{B}_{ek} \hat{\mathcal{F}} \hat{\tau}]^T \quad (55)$$

$$|y| = [|\dot{\delta}_r| |\dot{\delta}_{fw}| |\text{sign}(\dot{\delta}_{fw})| |\delta_{fw}|]. \quad (56)$$

Moreover, $\hat{\beta}_1$ and β_2 , ($\hat{\beta}_1, \beta_2 > 0$) are the fixed and adaptive gains used to control the convergence speed of AGFSMC, respectively, and $|u(t-1)|$ is the prior control input obtained at the time step $t-1$.

Therefore, the adaptation laws for updating the $\hat{a}(t)$ and $\hat{\beta}_1$ are designed as:

$$\dot{\hat{a}} = \Gamma |y|^T |s| \quad (57)$$

$$\dot{\hat{\beta}}_1 = |s| |u(t-1)|, \quad (58)$$

where Γ ($\Gamma > 0$) is the diagonal positive definite gain matrix used to tune the parameter adaptation speed. Figure 4 shows the framework of the proposed AGFSMC scheme.

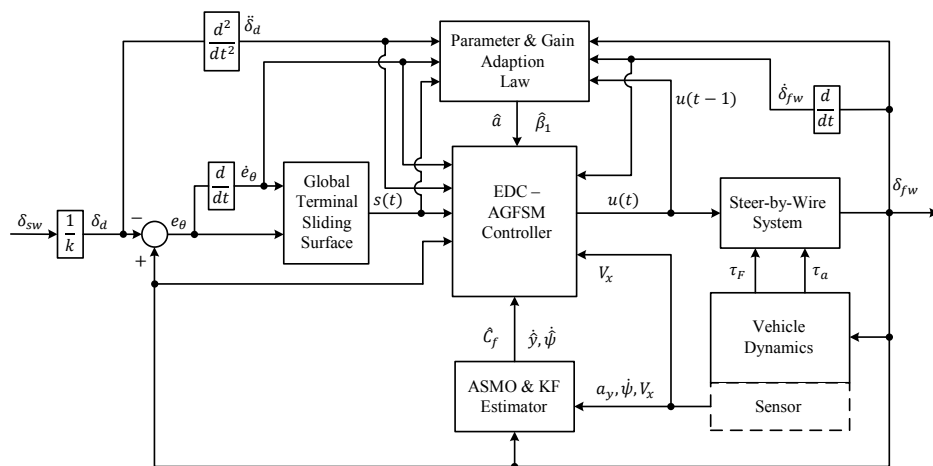


Figure 4. AGFSMC scheme framework.

Convergence Proof

The Lyapunov function candidate is defined as:

$$V_3 = \frac{1}{2}J_{ek}s^2 + \frac{1}{2}\tilde{a}^T\Gamma^{-1}\tilde{a} + \frac{1}{2}\tilde{\beta}_1^2, \quad (59)$$

where $\tilde{a}(t) = \hat{a}(t) - a$ is the parameter estimation error, $\tilde{\beta}_1(t) = \hat{\beta}_1(t) - \beta_1$ is the adaptive gain convergence error, and Γ^{-1} is the inverse of gain matrix.

The time derivative of Lyapunov function V_3 in terms of the SbW system (Equation (14)) and the control input (Equation (50)), with the considerations that $\dot{a} = 0$, $\dot{\beta}_1 = 0$, are obtained as follows:

$$\begin{aligned} \dot{V}_3 &= sJ_{ek}\dot{s} + \dot{\tilde{a}}^T\Gamma^{-1}\tilde{a} + \tilde{\beta}_1\dot{\beta}_1 \\ &= s[-J_{ek}\ddot{\delta}_r - B_{ek}\dot{\delta}_{fw} - \tau_{Fk} - \tau_{ak} + u] + \dot{\tilde{a}}^T\Gamma^{-1}\tilde{a} + \tilde{\beta}_1\dot{\beta}_1 \\ &= s[-J_{ek}\ddot{\delta}_r - B_{ek}\dot{\delta}_{fw} - \tau_{Fk} - \tau_{ak} - \text{sign}(s)(|\zeta\tau_{Fk}| \\ &\quad + |\zeta\tau_{ak}|) + u_A] + \dot{\tilde{a}}^T\Gamma^{-1}\tilde{a} + \tilde{\beta}_1\dot{\beta}_1 \\ &= s[-J_{ek}\ddot{\delta}_r - B_{ek}\dot{\delta}_{fw} + u_A] - (s\tau_{Fk} + |s||\zeta\tau_{Fk}|) \\ &\quad - (s\tau_{ak} + |s||\zeta\tau_{ak}|) + \dot{\tilde{a}}^T\Gamma^{-1}\tilde{a} + \tilde{\beta}_1\dot{\beta}_1 \\ &\leq s[-J_{ek}\ddot{\delta}_r - B_{ek}\dot{\delta}_{fw} + u_A] - |s|(|\zeta\tau_{Fk}| - |\tau_{Fk}|) \\ &\quad - |s|(|\zeta\tau_{ak}| - |\tau_{ak}|) + \dot{\tilde{a}}^T\Gamma^{-1}\tilde{a} + \tilde{\beta}_1\dot{\beta}_1. \end{aligned} \quad (60)$$

It is considered that $|\zeta\tau_{Fk}| < \tau_{Fk}$ and $|\zeta\tau_{ak}| < \tau_{ak}$, such that:

$$|\zeta\tau_{Fk}| - |\tau_{Fk}| = -\mathcal{F}|\text{sign}(\dot{\delta}_{fw})| \quad (61)$$

$$|\zeta\tau_{ak}| - |\tau_{ak}| = -\mathcal{T}\left(\left|\delta_{fw}\right| + \left|\frac{\dot{y} + l_f\dot{\psi}}{V_x}\right|\right), \quad (62)$$

where \mathcal{F} and \mathcal{T} are the uncertain residual parameters of frictional torque and self-aligning torque, respectively.

Substituting Equations (61), (63) and AGFSMC u_A (Equation (54)) into (Equation (60)), then the inequality is written as:

$$\begin{aligned} \dot{V}_3 &\leq s[-J_{ek}\ddot{\delta}_r - B_{ek}\dot{\delta}_{fw} - \text{sign}(s)\{\hat{J}_{ek}|\ddot{\delta}_r| + \hat{B}_{ek}|\dot{\delta}_{fw}| \\ &\quad + \hat{\mathcal{T}}|\delta_{fw}| + \hat{\mathcal{T}}\left|\frac{\dot{y} + l_f\dot{\psi}}{V_x}\right| + \hat{\beta}_1|u(t-1)|\} - \beta_2s] \\ &\quad + |s|\mathcal{F}|\text{sign}(\dot{\delta}_{fw})| + |s|\mathcal{T}|\delta_{fw}| + |s|\mathcal{T}\left|\frac{\dot{y} + l_f\dot{\psi}}{V_x}\right| \\ &\quad + \dot{\tilde{a}}^T\Gamma^{-1}\tilde{a} + \tilde{\beta}_1\dot{\beta}_1 \\ &= -(|s|\hat{J}_{ek}|\ddot{\delta}_r| + sJ_{ek}\ddot{\delta}_r) - (|s|\hat{B}_{ek}|\dot{\delta}_{fw}| + sB_{ek}\dot{\delta}_{fw}) \\ &\quad - (|s|\hat{\mathcal{F}}|\text{sign}(\dot{\delta}_{fw})| - s|\mathcal{F}|\text{sign}(\dot{\delta}_{fw})|) \\ &\quad - (|s|\hat{\mathcal{T}}|\delta_{fw}| - |s|\mathcal{T}|\delta_{fw}|) + |s|\mathcal{T}\left|\frac{\dot{y} + l_f\dot{\psi}}{V_x}\right| - |s|\hat{\mathcal{T}}\left|\frac{\dot{y} + l_f\dot{\psi}}{V_x}\right| \\ &\quad - |s|\hat{\beta}_1|u(t-1)| - \beta_2s^2 + \dot{\tilde{a}}^T\Gamma^{-1}\tilde{a} + \tilde{\beta}_1\dot{\beta}_1 \\ &= -|s||\ddot{\delta}_r|\tilde{J}_{ek} - |s||\dot{\delta}_{fw}|\tilde{B}_{ek} - |s||\text{sign}(\dot{\delta}_{fw})|\tilde{\mathcal{F}} - |s||\delta_{fw}|\tilde{\mathcal{T}} \\ &\quad - |s|\left(\hat{\mathcal{T}}\left|\frac{\dot{y} + l_f\dot{\psi}}{V_x}\right| - \mathcal{T}\left|\frac{\dot{y} + l_f\dot{\psi}}{V_x}\right|\right) - |s|\hat{\beta}_1|u(t-1)| - \beta_2s^2 \\ &\quad + \dot{\tilde{a}}^T\Gamma^{-1}\tilde{a} + \tilde{\beta}_1\dot{\beta}_1 \\ &= -|s||\ddot{y}|\tilde{a} + \dot{\tilde{a}}^T\Gamma^{-1}\tilde{a} - |s|\left(\hat{\mathcal{T}}\left|\frac{\dot{y} + l_f\dot{\psi}}{V_x}\right| - \mathcal{T}\left|\frac{\dot{y} + l_f\dot{\psi}}{V_x}\right|\right) \\ &\quad - |s|\hat{\beta}_1|u(t-1)| + (\hat{\beta}_1 - \beta_1)\dot{\beta}_1 - \beta_2s^2. \end{aligned} \quad (63)$$

With the adaptation laws of \hat{a} (Equation (57)) and $\hat{\beta}_1$ (Equation (58)), substituting into Equation (63) satisfies:

$$\dot{V}_3 \leq -|s| \left(\hat{\mathcal{T}} \left| \frac{\dot{y} + l_f \hat{\psi}}{V_x} \right| - \mathcal{T} \left| \frac{\dot{y} + l_f \psi}{V_x} \right| \right) - |s| \beta_1 |u(t-1)| - \beta_2 s^2 \quad (64)$$

The convergence proof shows that the proposed AGFSMC is stable and the inequality (Equation (64)) ensures that the global fast terminal sliding surface variable exponentially converges to zero ($s = 0$) in the finite time.

Remark 3. The signum function $\text{sign}(s)$ incorporates the chattering and discontinuity in the proposed controller. Therefore, to eliminate the chattering phenomenon the signum function is replaced by the boundary layer saturation function $\text{sat}(\cdot)$ such that Equations (51) and (53) are re-written as:

$$u_E = -\text{sat}(s)(|\xi \tau_{ak}| + |\xi \tau_{Fk}|) \quad (65)$$

$$u_A = -\text{sat}(s) \left(|\mathbb{Y}| \hat{a} + \hat{\mathcal{T}} \left| \frac{\dot{y} + l_f \hat{\psi}}{V_x} \right| + \hat{\beta}_1 |u(t-1)| \right) - \beta_2 s. \quad (66)$$

The boundary layer saturation function is defined as:

$$\text{sat}(s) = \begin{cases} \frac{s}{\phi} & |s| < \phi \\ \text{sign}(s) & \text{otherwise} \end{cases}, \quad (67)$$

where $\phi > 0$ represents the boundary layer thickness. Due to the boundary layer, the closed-loop error cannot converge to zero. However, a carefully selected value of ϕ would lead the error to a user-specified bounded region.

Remark 4. In order to avoid overestimation of \hat{a} and $\hat{\beta}_1$, which can lead the control input $u(t)$ to saturation, Equations (57) and (58) can be re-written for the permissible bounds of e_θ using the discontinuous projection mapping [36] as follows:

$$\dot{\hat{a}} = \begin{cases} 0 & \text{if } |e_\theta| \leq \varepsilon_4 \\ \Gamma |\mathbb{Y}|^T |s| & \text{otherwise} \end{cases} \quad (68)$$

$$\dot{\hat{\beta}}_1 = \begin{cases} 0 & \text{if } |e_\theta| \leq \varepsilon_5 \\ |s| |u(t-1)| & \text{otherwise} \end{cases}, \quad (69)$$

where ε_4 and ε_5 are defined as dead zone bounds [27] in terms of tracking error. Therefore, when the tracking error converges to the respective dead zone bound, the adaption mechanism will be switched off and after that \hat{a} and $\hat{\beta}_1$ become constant.

6. Simulation Results

In this section, the estimation accuracy of vehicle states and cornering stiffness coefficients, and the control input performance of the proposed AGFSMC scheme for SbW system road vehicles, are validated over the three different maneuvering tests, in comparison with adaptive sliding mode control (ASMC) and adaptive fast sliding mode control (ATSMC).

The first test (test 1) is sinusoidal maneuvering with varying tire–road conditions—snowy for the first 30 s and a dry asphalt road for the next 30 s—with the selected coefficient of friction as $\mu_{t<30} = 0.45$, $\mu_{t\geq 30} = 0.85$ and the tire cornering stiffness coefficients for the front and rear wheels as $C_{f(t<30)} = 4000$, $C_{f(t\geq 30)} = 8000$, $C_{r(t<30)} = 5000$, $C_{r(t\geq 30)} = 10,000$, respectively. The second test (test 2) is known as circular maneuvering, conducted over a dry asphalt road. Moreover, a high speed cornering test (test 3) is also introduced to further evaluate the robustness of the proposed scheme.

It is worth noting that the first two tests are carried out at longitudinal speed $V_x = 10$ m/s and the third test at $V_x = 20$ m/s with the same sampling rate of $\Delta T = 0.001$ s. Furthermore, the vehicle and SbW system parameters are listed in Table 2.

Table 2. Vehicle and SbW system parameters.

Parameter	Value (s)
m (kg)	1270
I_z (kg·m ²)	1537
l_f, l_r (m)	1.015, 1.895
J_{ek}	0.28
B_{ek}	0.88
k	18
t_m, t_p (m)	0.023, 0.016

The parameters for the proposed cooperative ASMO and KF estimator with the termination bounds are selected as: $\hat{L}_1(0) = \hat{L}_2(0) = 8, \rho_1 = \rho_2 = 10, \sigma = 0.001, \varepsilon_1 = \varepsilon_2 = 0.005, \varepsilon_3 = 0.01, m_0 = 1150$ kg, $I_{z0} = 1430$ kg·m², $\hat{w}_0 = [100 \ 100]^T$, $P_0 = 10000 \times I_{2 \times 2}$, $Q = (1 \times 10^{-6}) I_{2 \times 2}$, and $r_s = 0.001$.

In addition, the parameters for the designed AGFSMC scheme with dead zone bounds are chosen as: $\lambda_1 = \lambda_2 = 12, p = 7, q = 5, \phi = 0.8, \beta_2 = 4, t_{p0} = t_m = 0.016$ m, $\mu_o = 0.6, k_o = 16, \Gamma = I_{4 \times 4}$, $\varepsilon_4 = \varepsilon_5 = 0.002$, and the initial conditions are considered as $\hat{a}(0) = \hat{\beta}_1(0) = 0$.

To compare the performance of the proposed AGFSMC scheme with the adaptive sliding mode control (ASMC), as designed in [25], we used the following equations:

$$\begin{aligned}
 u &= \frac{1}{k}(J_{e0}(\lambda \dot{e} + \ddot{\delta}_d) + B_{e0}\dot{\delta}_{fw} + \xi_{f0}\text{sign}(\dot{\delta}_{fw}) + \omega s + K\text{sat}(s) + \hat{\rho}_\tau \tanh(\delta_{fw})) \\
 K &= 0.1(J_{e0}(\lambda|\dot{e}| + |\ddot{\delta}_d|) + B_{e0}|\dot{\delta}_{fw}| + \xi_{f0}) \\
 \dot{\hat{\rho}}_\tau &= \mu \frac{\omega}{J_{e0}} + \mu s \tanh(\delta_{fw}),
 \end{aligned} \tag{70}$$

where the tracking error $e = \delta_d - \delta_{fw}$ and the sliding surface $s = \dot{e} + \lambda e$ with $\dot{s} = (s_k - s_{k-1})/\Delta t$ are defined in Equation (71). The saturation function $\text{sat}(\cdot)$ is also taken to be the same as Equation (67) with boundary layer thickness $\phi = 0.8$. Moreover, the nominal SbW system parameters $J_{e0} = 3$, $B_{e0k} = 12$, $\xi_{f0} = 100$, $k = 18$, and the control parameters $\lambda = 12$, $\omega = 72$, $\mu = 450$ are selected according to the methodology defined in [25].

For performance comparison with ATSMC, as designed as [27], the calculations are given as follows:

$$\begin{aligned}
 u &= -\text{sat}(s) \left[\hat{a}_1 \left(\ddot{\delta}_d \right) + \hat{b}_1 |\dot{\delta}_{fw}| + \hat{c}_0 + \hat{c}_1 |\delta_{fw}| + \hat{c}_2 |\dot{\delta}_{fw}| + \lambda \hat{a}_p^{\frac{q}{p}}(e) \left(\frac{q}{p} - 1 \right) |\dot{e}| \right] - \frac{\hat{\rho}}{2} s \\
 &\quad - k_1 \text{sign}(s) - k_2 s \\
 \dot{\hat{c}}_0 &= \eta_1 |s| (1 - \sigma \hat{c}_0) \\
 \dot{\hat{c}}_1 &= \eta_2 |s| |\delta_{fw}| (1 - \sigma \hat{c}_1) \\
 \dot{\hat{c}}_2 &= \eta_3 |s| |\dot{\delta}_{fw}| (1 - \sigma \hat{c}_2) \\
 \dot{\hat{a}}_1 &= \left(\eta_4 |s| \left(\ddot{\delta}_d \right) + \eta_4 |s| \lambda \frac{q}{p} (e) \left(\frac{q}{p} - 1 \right) |\dot{e}| \right) (1 - \sigma \hat{a}_1) \\
 \dot{\hat{b}}_1 &= \eta_5 |s| |\dot{\delta}_{fw}| (1 - \sigma \hat{b}_1), \dot{\hat{\rho}} = \eta_6 \frac{s^2}{2} (1 - \sigma \hat{\rho}),
 \end{aligned} \tag{71}$$

where $\lambda, p, q, \text{sat}(s)$, and ϕ have the same values as those defined in AGFSMC. Moreover, the control parameters and adjustable parameters for adaptive laws are selected according to [27] as follows: $\eta_1 = 4, \eta_2 = \eta_3 = \eta_4 = \eta_5 = \eta_6 = 2, k_1 = 0.001, k_2 = 4, \ddot{\delta}_d = 2$ and $\rho = 0.001$, respectively.

6.1. Sinusoidal Maneuvering Test (Test 1)

The reference steering wheel angle is generated by:

$$\delta_d = 0.4 \sin(0.5\pi t) \text{ rad.} \quad (72)$$

Figure 5 shows the simultaneously estimated lateral velocity, yaw rate, and cornering stiffness coefficients. It is observed that the cooperative ASMO and KF scheme intelligently cope with the tire–road variations and estimate the vehicle states and cornering stiffness coefficients by self-tuning the gains according to the driving environment. Figure 5c shows that the estimated \hat{C}_f, \hat{C}_r have not only converged to the neighborhood of the actual values in both dry and snowy conditions, but also become constant after the condition e_3 reached a specified termination bound.

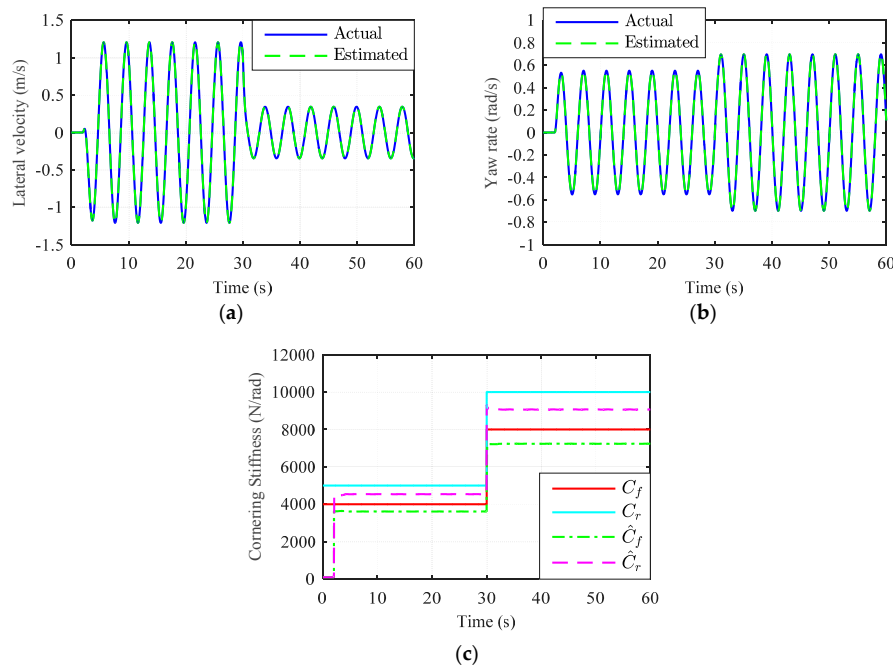


Figure 5. Estimation results of vehicle states and cornering stiffness coefficients in test 1: (a) Estimated lateral velocity; (b) Estimated yaw rate; (c) Estimated cornering stiffness coefficients.

Figure 6 represents the tracking response and the control input performance of the AGFSMC scheme against the varying tire–road disturbance forces. We can see from Figure 6b that the proposed methodology effectively eliminates the impact of self-aligning torque (Equation (20)) and Coulomb frictional torque (Equation (21)) from the SbW system and ensures that the front wheels are precisely tracking the reference steering angle with a steady state tracking error of 0.002 rad. It is noted that at the beginning of sinusoidal maneuvering, after 3 s, the tracking error reached the peak value of 0.01 rad. This is because we started all the parameter estimations from very low values, such as $\hat{w}_0 = [100 \ 100]^T$, $\hat{a}(0) = \hat{\beta}_1(0) = 0$. Therefore, right after the peak error, all the estimated parameters converged to the sufficient estimation set. As a result, the peak tracking error also converged to the steady-state dead zone region.

Moreover, Figure 7 shows the estimated SbW system parameters and the sliding gain adaptation profile. It is observed that the estimated SbW system parameters did not converge to the listed actual constants, but due to the adaptive capability of the proposed control scheme, all parameters as well as the sliding gain are adaptively adjusted in time for both driving conditions, which ensure the closed-loop stability of the SbW system. Hence, the outstanding steering performance of the SbW

system vehicle is achieved against the nonlinear tire–road disturbance forces and the uncertain SbW system parameters.

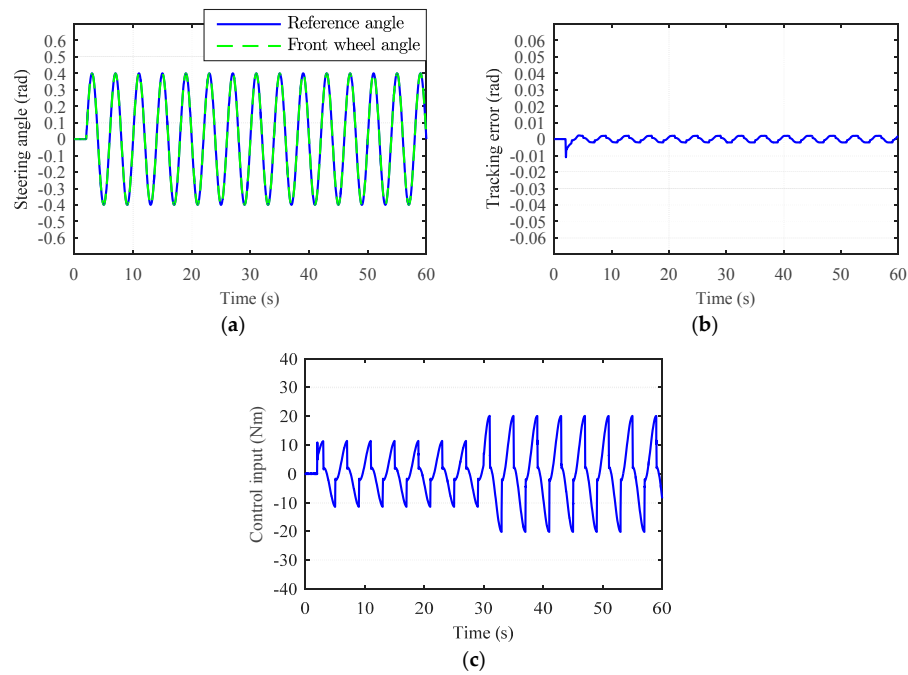


Figure 6. Control performance of the proposed AGFSMC scheme in test 1: (a) Tracking performance; (b) Tracking error; (c) Control input torque.

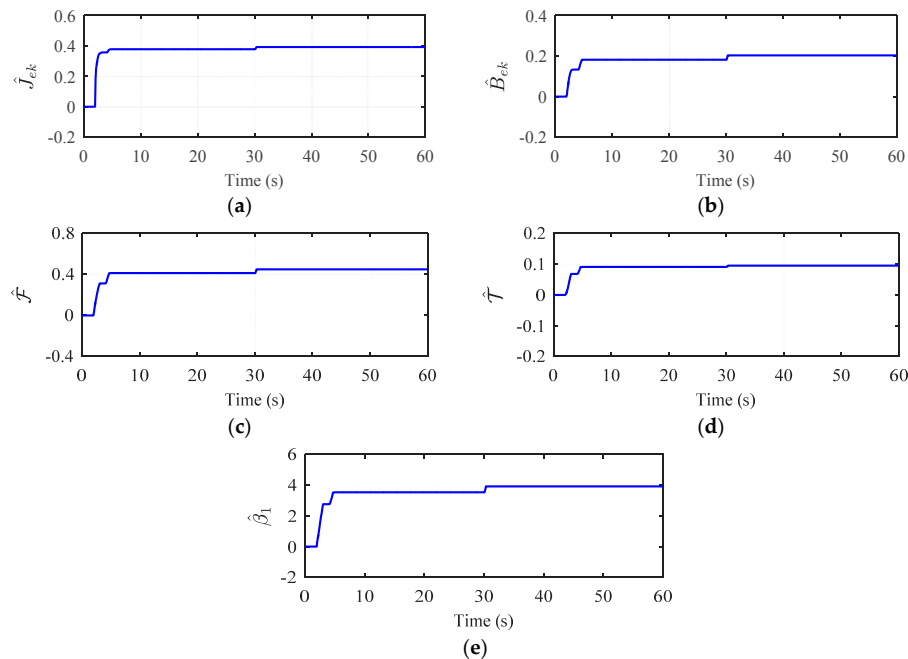


Figure 7. Estimated SbW system parameters and sliding gain with AGFSMC scheme in test 1: (a–d) Estimated SbW system parameters; (e) Estimated sliding gain.

Figure 8 demonstrates that the steering performance of the ASMC scheme is not as good as that of the proposed AGFSMC scheme. This is because the hyperbolic tangent function used in ASMC is unable to replicate the actual self-aligning torque acting on the SbW system. Also, the adaptation law

cannot estimate the appropriate equivalent coefficient of self-aligning torque to compensate for the varying tire–road conditions. Consequently, the overall tracking error is much higher, particularly in the dry asphalt road condition: the tracking error peaks to the steady-state value of 0.06 rad, which is almost 30 times higher than in the proposed scheme. Although the ASMC scheme has the information of nominal parameters and utilized the saturation function, it incorporates high-frequency chattering during the first 3 s of the simulation, where the reference angle is set to zero.

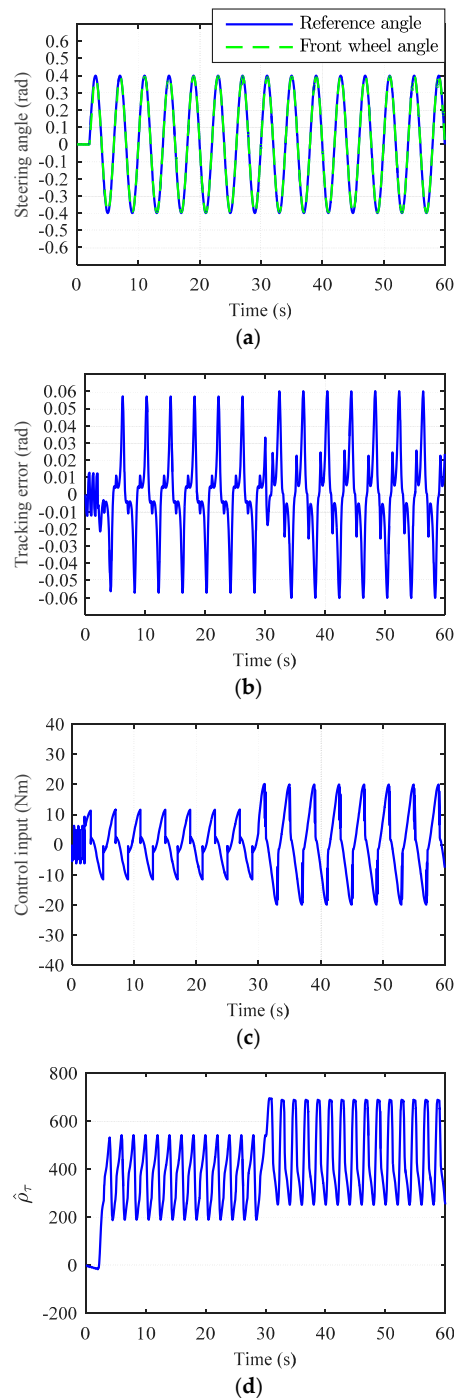


Figure 8. Control performance of adaptive sliding mode controller in test 1: (a) Tracking performance; (b) Tracking error; (c) Control input torque; (d) Estimated equivalent coefficient of self-aligning torque.

Figure 9 shows that the overall tracking response of ATSMC is better than the ASMC under the varying driving conditions, while both schemes cannot outperform the proposed AGFSMC. It can be seen that the control input overshoots the allowable control limit, which causes irregular spikes in the tracking error. We noticed two reasons for that: (1) The designed adaptation law for estimating the control parameter \hat{a}_1 does not include a provision to maintain the positive estimation; and (2) the ATSMC does not possess any mechanism to bound or stop the parameter adaptation process for avoiding overestimations, as compared to the one proposed in AGFSMC. Therefore, the tracking error is consistently converging to a smaller region with spikes due to the large and continuous parameter estimation, which may lead the controller to saturation state.

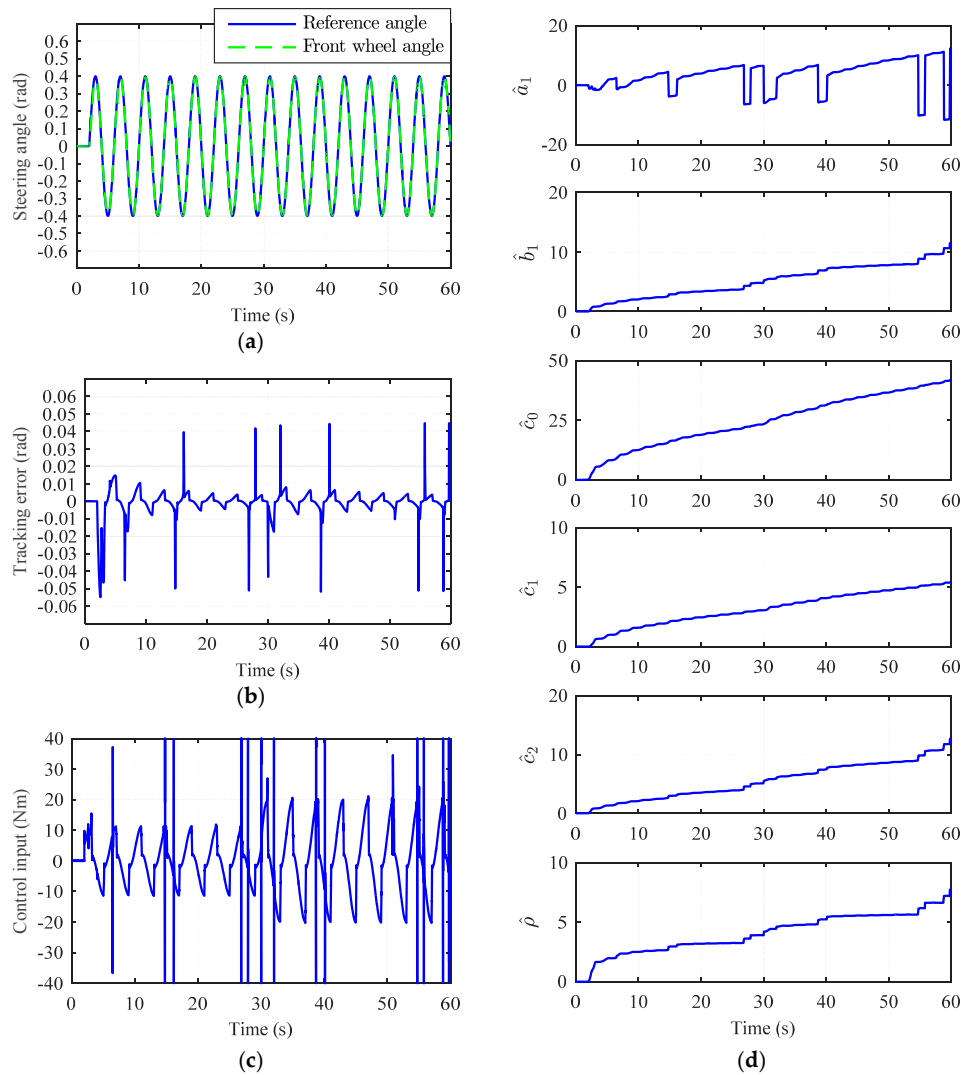


Figure 9. Control performance of adaptive terminal sliding mode control in test 1: (a) Tracking performance; (b) Tracking error; (c) Control input torque; (d) Estimated parameters.

6.2. Circular Maneuvering Test (Test 2)

The circular maneuvering test is carried out over the dry asphalt road for 25 s with these selected tire–road parameters: $C_f = 8000$, $C_r = 10000$, and $u = 0.85$.

Figures 10–12 portray the promising results of the proposed AGFSMC scheme in all aspects during test 2. We can see the fine estimation of vehicle states and cornering coefficients in Figure 10. The estimated cornering coefficients takes less than a second to converge to the sufficient estimation set over the dry asphalt, such as, $\hat{C}_f \cong 7250$, $\hat{C}_r \cong 9050$, and becomes constant after e_3 satisfies the

selected ε_3 bound. Thus, Figure 11 exhibits the excellent tracking response of the front wheels with an observed peak tracking error of 0.008 rad, which eventually converged to the ε_4 bound after the rapid adjustment of all adaptive parameters \hat{f}_{ek} , \hat{b}_{ek} , $\hat{\mathcal{F}}$, $\hat{\mathcal{T}}$, and $\hat{\beta}_1$ to certain constants, as shown in Figure 12.

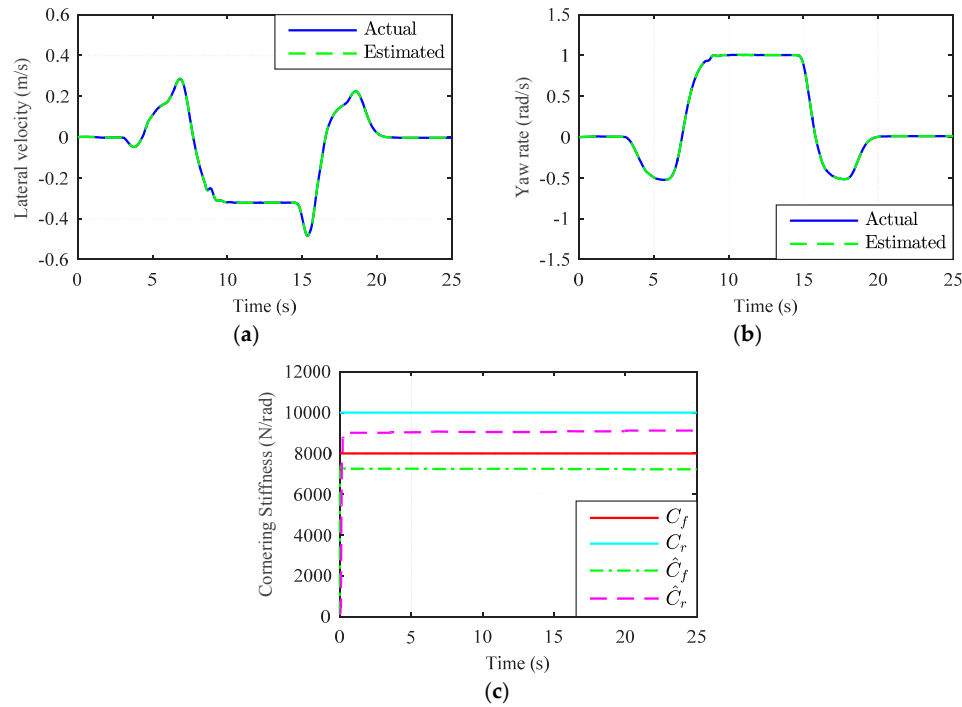


Figure 10. Estimation results of vehicle states and cornering stiffness coefficients in test 2: (a) Estimated lateral velocity; (b) Estimated yaw rate; (c) Estimated cornering stiffness coefficients.

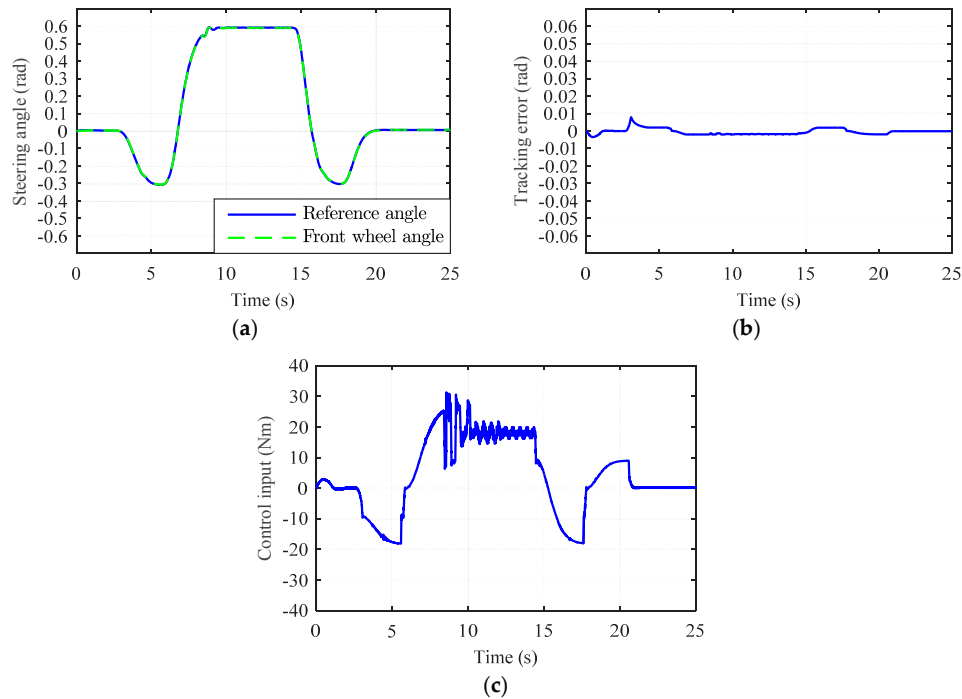


Figure 11. Control performance of the proposed AGFSMC scheme in test 2: (a) Tracking performance; (b) Tracking error; (c) Control input torque.

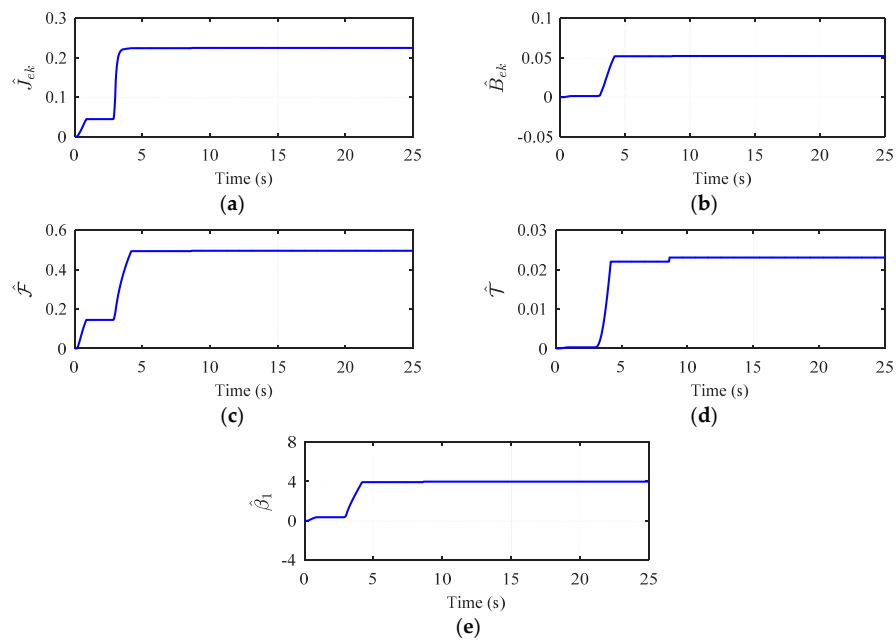


Figure 12. Estimated SbW system parameters and sliding gain with AGFSMC scheme in test 2: (a–d) Estimated SbW system parameters; (e) Estimated sliding gain.

In contrast to the proposed scheme, the ASMC shows the worst tracking performance throughout test 2. It can be seen from Figure 13 that the tracking error is unable to obtain any steady state bound and reached a peak value of 0.076 rad, which is almost 9.5 times higher than in the proposed AGFSMC scheme. Moreover, the adaptation law also shows inconsistent behavior in the last 7 s of this test, where the estimated coefficient of self-aligning torque rapidly drops to a highly negative value. As a result, neither tracking error nor sliding surface converged to the steady state boundary at a finite time in the Lyapunov's sense.

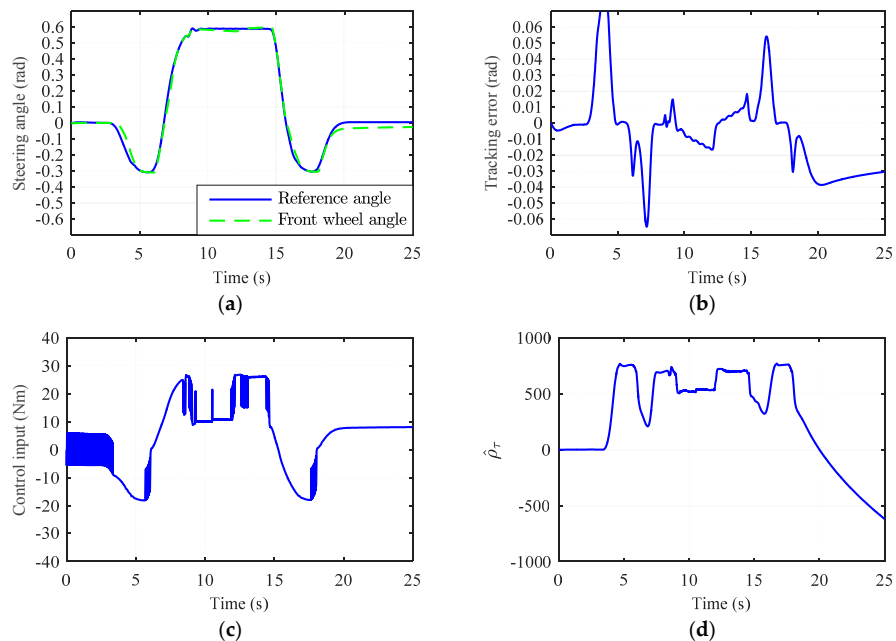


Figure 13. Control performance of adaptive sliding mode controller in test 2: (a) Tracking performance; (b) Tracking error; (c) Control input torque; (d) Estimated equivalent coefficient of self-aligning torque.

On the other hand, the ATSMC performed slightly better than the ASMC in terms of tracking response and also managed to converge the tracking error to the steady state bound during test 2. The peak tracking error observed under the ATSMC scheme is 0.067 rad as shown in Figure 14, which is marginally less than the ASMC but almost 8.35 times higher than the proposed scheme. Moreover, the abrupt shift in $\hat{\alpha}_1$ parameter estimation and the multiple control input overshoots are again observed in this test.

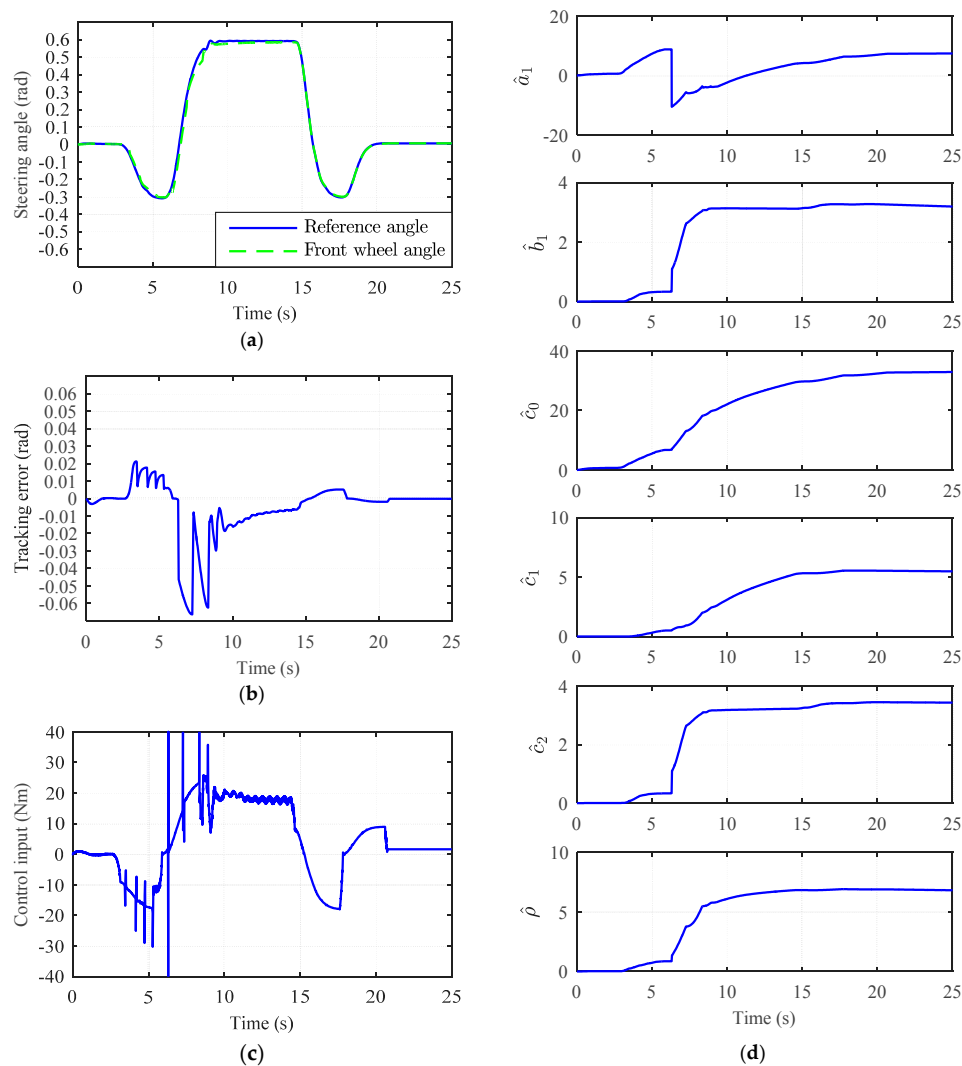


Figure 14. Control performance of adaptive terminal sliding mode control in test 2: (a) Tracking performance; (b) Tracking error; (c) Control input torque; (d) Estimated parameters.

6.3. High Speed Cornering Test (Test 3)

In order to further evaluate the estimation accuracy, tracking response, and control input performance of the proposed AGFSMC scheme, a high-speed cornering test is performed on a dry asphalt road for 45 s.

As expected, Figures 15–17 clearly indicate the remarkable performance of the proposed scheme against the parametric uncertainties and tire–road disturbance. The cooperative ASMO and KF also maintain the robustness and provide adequate estimated dynamics to stabilize the effect of self-aligning torque and frictional torque at high speed. The peak tracking error observed during test 3 under the AGFSMC scheme is 0.0095 rad, which is almost eight times lower than ASMC (0.076 rad), and four times lower than ATSMC (0.04 rad). Compared to other control schemes, Figure 18 shows that the

tracking error under ASMC was again unable to attain any steady state bound and also incorporates high-frequency chattering at constant steering angle inputs. The ATSMC shows a decent performance regarding the tracking error convergence as compared to ASMC. However, the sudden parameter estimation shift with control overshoot still exists in this test, as shown in Figure 19.

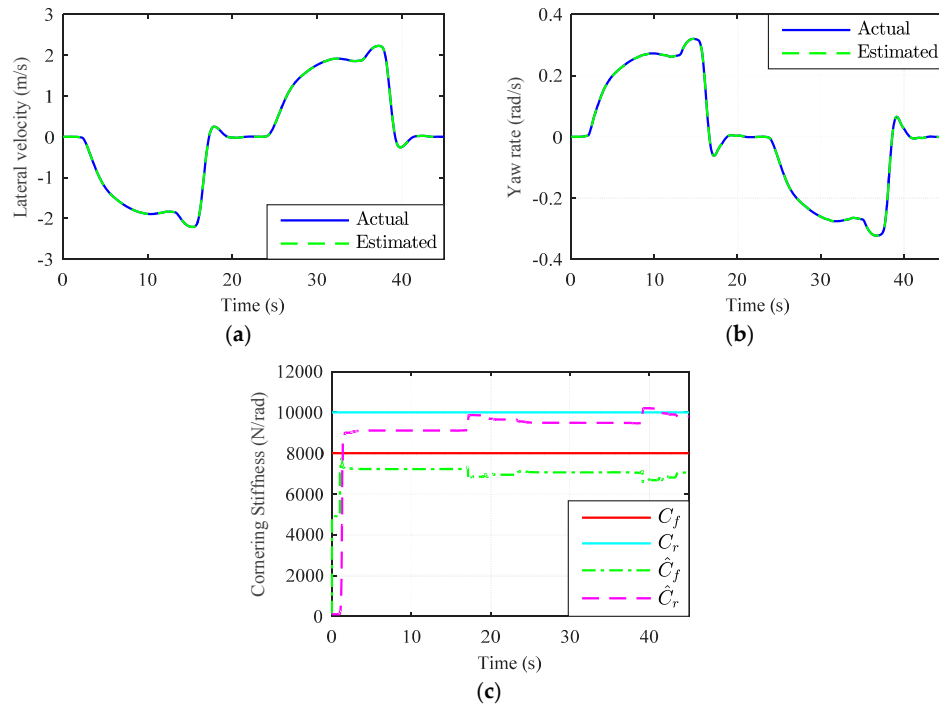


Figure 15. Estimation results of vehicle states and cornering stiffness coefficients in test 3: (a) Estimated lateral velocity; (b) Estimated yaw rate; (c) Estimated cornering stiffness coefficients.

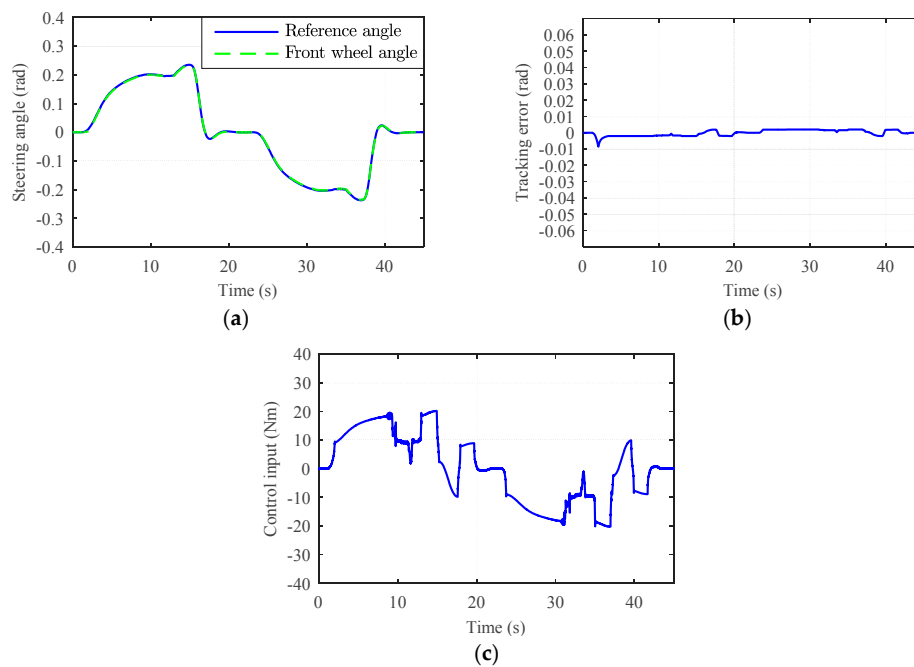


Figure 16. Control performance of the proposed AGFSMC scheme in test 3: (a) Tracking performance; (b) Tracking error; (c) Control input torque.

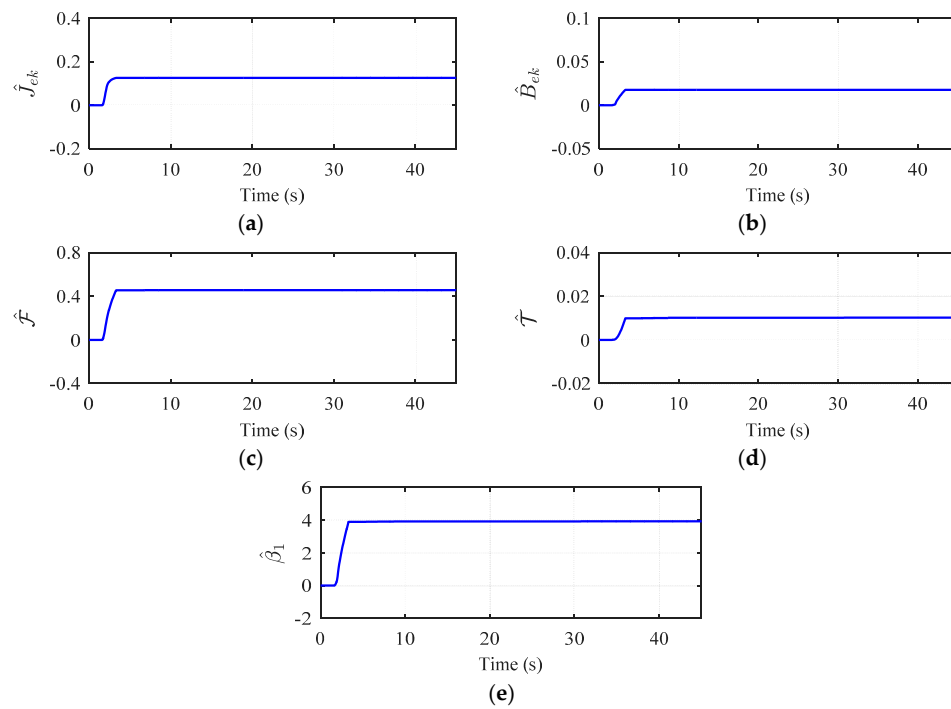


Figure 17. Estimated SbW system parameters and sliding gain with AGFSMC scheme in test 3: (a–d) Estimated SbW system parameters; (e) Estimated sliding gain.

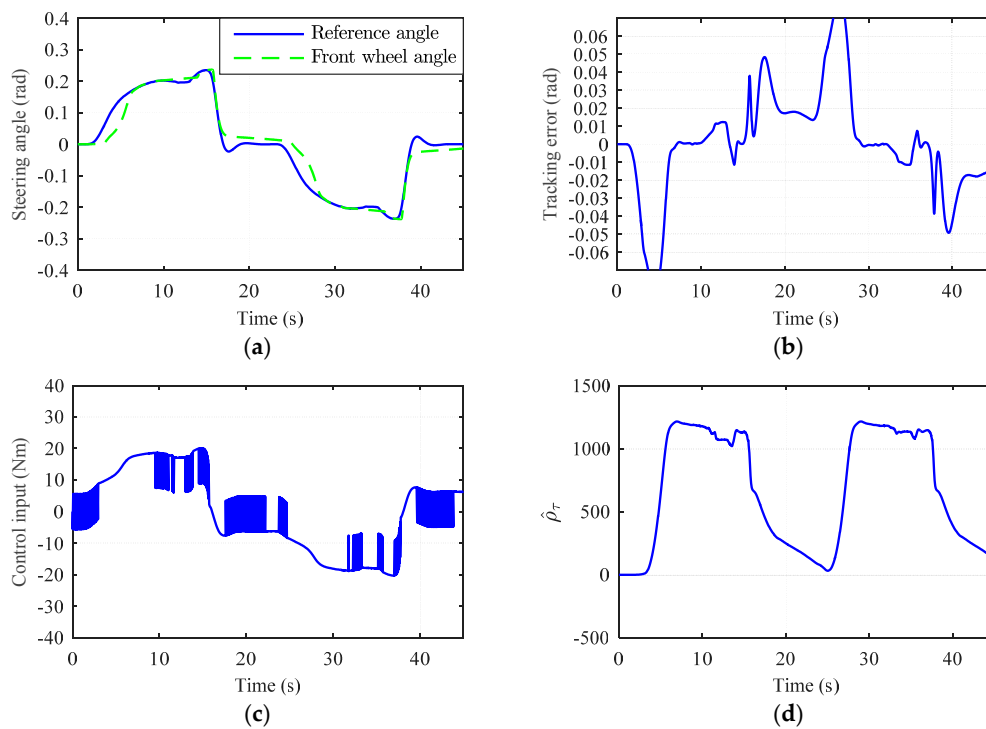


Figure 18. Control performance of adaptive sliding mode controller in test 3: (a) Tracking performance; (b) Tracking error; (c) Control input torque; (d) Estimated equivalent coefficient of self-aligning torque.

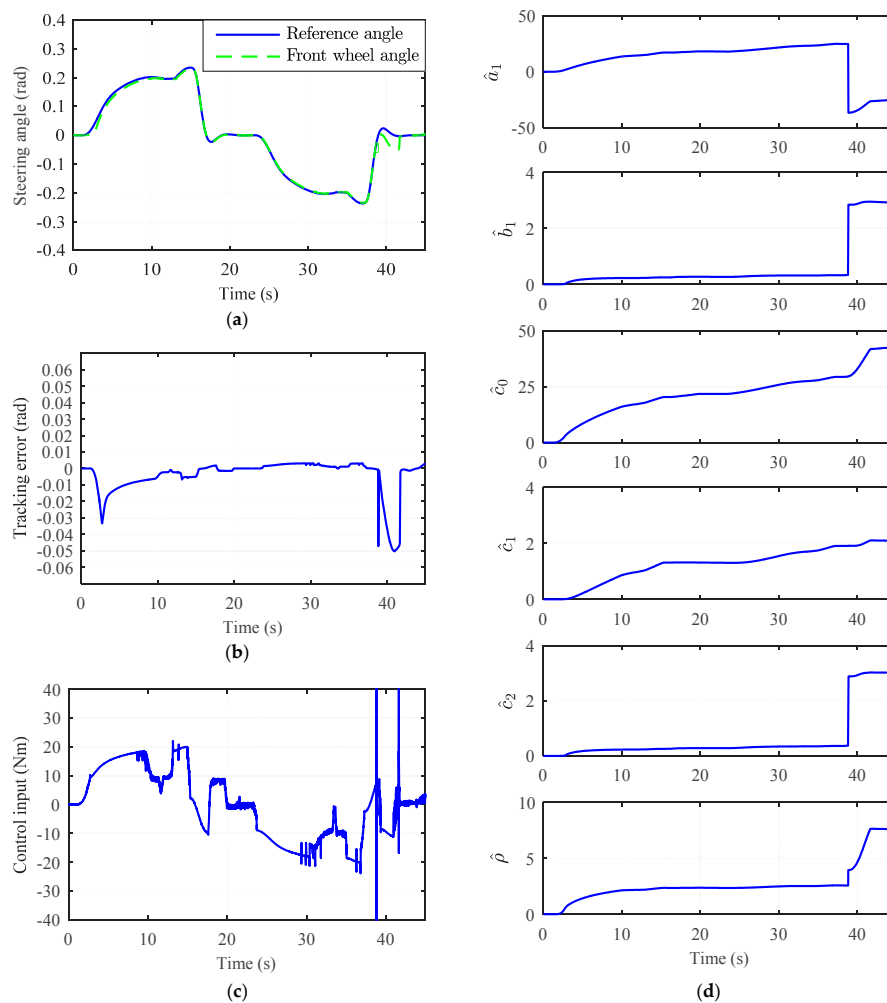


Figure 19. Control performance of adaptive terminal sliding mode control in test 3: (a) Tracking performance; (b) Tracking error; (c) Control input torque; (d) Estimated parameters.

7. Conclusions

In this paper, we have developed an AGFSMC scheme for SbW system road vehicles with unknown steering parameters. It has been demonstrated that the cooperative ASMO and KF intelligently cope with tire–road variations and simultaneously provide the best set of estimated vehicle states and cornering stiffness coefficients. Thereafter, the estimated dynamics-based AGFSMC is designed to adapt to the unknown SbW system parameters and eliminate the effect of tire–road disturbance forces. The proposed global fast terminal sliding surface guarantees the precise tracking of front wheels and ensures the asymptotic convergence of tracking error. Finally, the comparative study results are analyzed as follows:

- The adaptive features of cooperative ASMO and KF showed strong robustness against varying driving conditions in all three maneuvering tests, and estimated the sufficient dynamics to stabilize the impact of tire–road frictional torque and self-aligning torque.
- The proposed AGFSMC is proven to attain a smaller peak tracking error and faster convergence of steady-state error to smaller bounds in comparison with ASMC and ATSMC over all three maneuvers.
- The discontinuous projection mapping along with designed dead zones, also effectively managed to restrict the estimation drift problem.

Thus, the comparative study validates the remarkable steering performance of the proposed AGFSMC scheme, carried out over three different driving maneuvers. For our forthcoming work, we will investigate the dynamic behavior of nonlinear self-aligning torque and Coulomb frictional torque in extreme maneuvering conditions. In addition, we are also investigating the adaptive second-order sliding mode control for SbW system road vehicles to improve the estimation accuracy of dynamic tire–road disturbance forces under varying driving conditions.

Acknowledgments: This research was partially supported by the Higher Education Commission of Pakistan by the award letter No. HRDI-UESTPs/Batch-II/South Korea/2012.

Author Contributions: Junaid Iqbal proposed the idea, implemented it by simulations and wrote the manuscript. Mian Ashfaq Ali contributed to comparative study analysis. Khalil Muhammad Zuhaib and Abdul Manan Khan made suggestions in the manuscript correction and improvements. Changsoo Han supervised the study and manuscript writing process.

Conflicts of Interest: The authors declare no conflict of interest.

Abbreviations

The following abbreviations are used in this article:

$V_x, V_y, \dot{\psi}$	Vehicle's velocities and yaw rate
$\ddot{y}, \ddot{\psi}$	Vehicle's lateral and yaw acceleration
m, I_z	Vehicle's mass and mass moment of inertia
F_{yf}, F_{yr}	Lateral force at front and rear wheel
F_{xf}, F_{xr}	Longitudinal force at front and rear wheel
C_f, C_r	Cornering coefficient of front and rear wheel
α_f, α_r	Sideslip angle of front and rear wheel
J_{fw}, J_{fm}, J_{eq}	Moment of inertia of front wheels, actuator, and equivalent SbW system
B_{fw}, B_{fm}, B_{eq}	Viscous damping of front wheels, actuator, and equivalent SbW system
l_f, l_r	Distance of front and rear axles from center of gravity
t_p, t_m	Pneumatic and mechanical trail
τ_F, τ_a	Tire–road frictional torque and self-aligning torque
μ	Tire–road coefficient of dry friction
F_{zf}	Vertical load on front axle
k	Steering ratio
$\dot{\hat{y}}, \dot{\hat{\psi}}$	ASMO estimated vehicle states
\hat{L}_1, \hat{L}_2	ASMO adaptive gains
ρ_1, ρ_2	ASMO adaptation law speed adjustment parameters
\hat{C}_f, \hat{C}_r	KF estimated cornering coefficients
e_1, e_2, e_3	ASMO and KF estimation errors
$\varepsilon_1, \varepsilon_2, \varepsilon_3$	ASMO and KF termination bounds
δ_{fw}	Front wheel angle
δ_d	Reference angle
e_θ	Tracking error
s	Sliding surface
$\lambda_1, \lambda_2, q, p$	GFTSM surface parameters
$\hat{J}_{ek}, \hat{B}_{ek}, \hat{\mathcal{F}}, \hat{\mathcal{T}}, \hat{\beta}_1, \beta_2$	AGFSM estimated and fast convergence parameters
$\varepsilon_4, \varepsilon_5$	AGFSM adaptation law dead zone bounds
u	AGFSM control input

References

1. SAE International Technical Standard Provides Terminology for Motor Vehicle Automated Driving Systems. Available online: <http://www.sae.org/autodrive> (accessed on 10 December 2016).
2. Federal Automated Vehicles Policy. Available online: <https://www.transportation.gov/AV> (accessed on 23 January 2017).

3. Ishida, S.; Gayko, J.E. Development, evaluation and introduction of a lane keeping assistance system. In Proceedings of the 2004 IEEE Intelligent Vehicles Symposium, Parma, Italy, 14–17 June 2004; pp. 943–944.
4. Hebert, M.H.; Thorpe, C.; Stentz, A. *Intelligent Unmanned Ground Vehicles*; Springer US: Boston, MA, USA, 1997.
5. Crane, C.D., III; Armstrong, D.G., II; Touchton, R.; Galluzzo, T.; Solanki, S.; Lee, J.; Kent, D.; Ahmed, M.; Montane, R.; Ridgeway, S.; et al. Team CIMAR's NaviGator: An unmanned ground vehicle for the 2005 DARPA grand challenge. *J. Field Robot.* **2006**, *23*, 599–623. [[CrossRef](#)]
6. How Google's Self-Driving Car Works—IEEE Spectrum. Available online: <http://spectrum.ieee.org/automaton/robotics/artificial-intelligence/how-google-self-driving-car-works> (accessed on 12 March 2016).
7. Gietelink, O.; Ploeg, J.; De Schutter, B.; Verhaegen, M. Development of advanced driver assistance systems with vehicle hardware-in-the-loop simulations. *Veh. Syst. Dyn.* **2006**, *44*, 569–590. [[CrossRef](#)]
8. 2014 Top Ten Tech Cars—IEEE Spectrum. Available online: <http://spectrum.ieee.org/transportation/self-driving/2014-top-ten-tech-cars> (accessed on 9 October 2016).
9. Top Tech Cars 2013: Infiniti Q50—IEEE Spectrum. Available online: <http://spectrum.ieee.org/transportation/advanced-cars/infiniti-q50> (accessed on 9 October 2016).
10. Wang, H.; Man, Z.; Shen, W.; Cao, Z.; Zheng, J.; Jin, J.; Tuan, D.M. Robust Control for Steer-by-Wire Systems with Partially Known Dynamics. *IEEE Trans. Ind. Inform.* **2014**, *10*, 2003–2015. [[CrossRef](#)]
11. Wang, H.; Xu, Z.; Do, M.T.; Zheng, J.; Cao, Z.; Xie, L. Neural-network-based robust control for steer-by-wire systems with uncertain dynamics. *Neural Comput. Appl.* **2015**, *26*, 1575–1586. [[CrossRef](#)]
12. Wang, H.; Man, Z.; Shen, W.; Zheng, J. Robust sliding mode control for Steer-by-Wire systems with AC motors in road vehicles. In Proceedings of the 2013 8th IEEE Conference on Industrial Electronics and Applications (ICIEA), Melbourne, VIC, Australia, 19–21 June 2013; pp. 674–679.
13. Wang, H.; Man, Z.; Kong, H.; Shen, W. Terminal sliding mode control for steer-by-wire system in electric vehicles. In Proceedings of the 2012 7th IEEE Conference on Industrial Electronics and Applications (ICIEA), Singapore, 18–20 July 2012; pp. 919–924.
14. Wang, H.; Kong, H.; Man, Z.; Tuan, D.M.; Cao, Z.; Shen, W. Sliding mode control for steer-by-wire systems with AC motors in road vehicles. *IEEE Trans. Ind. Electron.* **2014**, *61*, 1596–1611. [[CrossRef](#)]
15. Do, M.T.; Man, Z.; Zhang, C.; Wang, H.; Tay, F.S. Robust Sliding Mode-Based Learning Control for Steer-by-Wire Systems in Modern Vehicles. *IEEE Trans. Veh. Technol.* **2014**, *63*, 580–590. [[CrossRef](#)]
16. Iqbal, J.; Shin, K.; Han, C. Neural network based control for steer-by-wire systems vehicles. *Adv. Circuits Syst. Signal Process. Telecommun.* **2014**. Available online: <http://www.wseas.us/e-library/conferences/2015/Dubai/CSST/CSST-09.pdf> (accessed on 16 July 2017).
17. Kim, C.J.; Jang, J.H.; Yu, S.N.; Lee, S.H.; Han, C.S.; Hedrick, J.K. Development of a control algorithm for a tie-rod-actuating steer-by-wire system. *Proc. Inst. Mech. Eng. Part D* **2008**, *222*, 1543–1557. [[CrossRef](#)]
18. Park, T.J.; Han, C.S.; Lee, S.H. Development of the electronic control unit for the rack-actuating steer-by-wire using the hardware-in-the-loop simulation system. *Mechatronics* **2005**, *15*, 899–918. [[CrossRef](#)]
19. OH, S.W.; CHAE, H.C.; YUN, S.C.; HAN, C.S. The Design of a Controller for the Steer-by-Wire System. *JSME Int. J. Ser. C* **2004**, *47*, 896–907. [[CrossRef](#)]
20. Yih, P.; Gerdes, J.J.C. Modification of vehicle handling characteristics via steer-by-wire. *IEEE Trans. Control Syst. Technol.* **2005**, *13*, 965–976. [[CrossRef](#)]
21. Yamaguchi, Y.; Murakami, T. Adaptive Control for Virtual Steering Characteristics on Electric Vehicle Using Steer-by-Wire System. *IEEE Trans. Ind. Electron.* **2009**, *56*, 1585–1594. [[CrossRef](#)]
22. Polesel, M.; Shyrokau, B.; Tanelli, M.; Savitski, D.; Ivanov, V.; Ferrara, A. Hierarchical control of overactuated vehicles via sliding mode techniques. In Proceedings of the 2014 IEEE 53rd Annual Conference on Decision and Control (CDC), Los Angeles, CA, USA, 15–17 December 2014; pp. 4095–4100.
23. Janbakhsh, A.A.; Bayani Khaknejad, M.; Kazemi, R. Simultaneous vehicle-handling and path-tracking improvement using adaptive dynamic surface control via a steer-by-wire system. *Proc. Inst. Mech. Eng. Part D* **2012**, *227*, 345–360. [[CrossRef](#)]
24. Kazemi, R.; Janbakhsh, A.A. Nonlinear adaptive sliding mode control for vehicle handling improvement via steer-by-wire. *Int. J. Automot. Technol.* **2010**, *11*, 345–354. [[CrossRef](#)]
25. Sun, Z.; Zheng, J.; Man, Z.; Wang, H. Robust Control of a Vehicle Steer-by-Wire System Using Adaptive Sliding Mode. *IEEE Trans. Ind. Electron.* **2016**, *63*, 2251–2262. [[CrossRef](#)]
26. Sun, Z.; Zheng, J.; Wang, H.; Man, Z. Adaptive fast non-singular terminal sliding mode control for a vehicle steer-by-wire system. *IET Control Theory Appl.* **2017**, *11*, 1245–1254. [[CrossRef](#)]

27. Wang, H.; Man, Z.; Kong, H.; Zhao, Y.; Yu, M.; Cao, Z.; Zheng, J.; Do, M.T. Design and Implementation of Adaptive Terminal Sliding-Mode Control on a Steer-by-Wire Equipped Road Vehicle. *IEEE Trans. Ind. Electron.* **2016**, *63*, 5774–5785. [[CrossRef](#)]
28. Wenzel, T.A.; Burnham, K.J.; Blundell, M.V.; Williams, R.A. Dual extended Kalman filter for vehicle state and parameter estimation. *Veh. Syst. Dyn.* **2006**, *44*, 153–171. [[CrossRef](#)]
29. Hong, S.; Lee, C.; Borrelli, F. A novel approach for vehicle inertial parameter identification using a dual Kalman filter. *IEEE Trans. Intell. Transp. Syst.* **2015**, *16*, 151–161. [[CrossRef](#)]
30. Oh, J.J.; Choi, S.B. Vehicle velocity observer design using 6-D IMU and multiple-observer approach. *IEEE Trans. Intell. Transp. Syst.* **2012**, *13*, 1865–1879. [[CrossRef](#)]
31. Imsland, L.; Johansen, T.A.; Fossen, T.I.; Fjær Grip, H.; Kalkkuhl, J.C.; Suissa, A. Vehicle velocity estimation using nonlinear observers. *Automatic* **2006**, *42*, 2091–2103. [[CrossRef](#)]
32. Zhao, L.H.; Liu, Z.Y.; Chen, H. Design of a nonlinear observer for vehicle velocity estimation and experiments. *IEEE Trans. Control Syst. Technol.* **2011**, *19*, 664–672. [[CrossRef](#)]
33. Guo, H.; Chen, H.; Cao, D.; Jin, W. Design of a reduced-order non-linear observer for vehicle velocities estimation. *IET Control Theory Appl.* **2013**, *7*, 2056–2068. [[CrossRef](#)]
34. Du, J.; Liu, Z.; Wang, Y.; Wen, C. An adaptive sliding mode observer for lithium-ion battery state of charge and state of health estimation in electric vehicles. *Control Eng. Pract.* **2016**, *54*, 81–90. [[CrossRef](#)]
35. Woodman, O. *An Introduction to Inertial Navigation*; University of Cambridge: Cambridge, UK, 2007.
36. Xu, L.; Yao, B. Adaptive robust control of mechanical systems with non-linear dynamic friction compensation. *Int. J. Control* **2008**, *81*, 167–176. [[CrossRef](#)]
37. Slotine, J.; Li, W. *Applied Nonlinear Control*; Prentice Hall: Englewood Cliffs, NJ, USA, 1991.
38. Rajamani, R. *Vehicle Dynamics and Control*; Springer Science & Business Media: New York, NY, USA, 2011.
39. Abe, M. *Vehicle Handling Dynamics: Theory and Application*; Elsevier Science Technology: London, UK, 2015.
40. Benoussaad, M.; Sijobert, B.; Mombaur, K. Robust foot clearance estimation based on the integration of foot-mounted IMU acceleration data. *Sensors* **2016**, *16*. [[CrossRef](#)] [[PubMed](#)]
41. Simon, D. *Optimal State Estimation: Kalman, H Infinity, and Nonlinear Approaches*; Wiley-Interscience: Hoboken, NJ, USA, 2006.
42. Liu, J.; Wang, X. *Advanced Sliding Mode Control for Mechanical Systems: Design, Analysis and MATLAB Simulation*; Springer Science & Business Media: New York, NY, USA, 2012.



© 2017 by the authors. Licensee MDPI, Basel, Switzerland. This article is an open access article distributed under the terms and conditions of the Creative Commons Attribution (CC BY) license (<http://creativecommons.org/licenses/by/4.0/>).